The Meteoritical Society

Meteoritics & Planetary Science 56, Nr 3, 642–662 (2021)
doi: 10.1111/maps.13644

Noble gases in cluster chondrite clasts and their host breccias

Kim MÜSING[1], Henner BUSEMANN[1], Liliane HUBER[1], Colin MADEN[1], My E. I. RIEBE[1], Rainer WIELER[1*], and Knut METZLER[2]

[1]Department of Earth Sciences, Institute of Geochemistry and Petrology, ETH Zürich, Clausiusstrasse 25, CH-8092 Zürich, Switzerland
[2]Institut für Planetologie, University of Münster, Wilhelm-Klemm-Str. 10, 48149 Münster, Germany
[*]Corresponding author. E-mail: wieler@erdw.ethz.ch

(Received 04 December 2020; revision accepted 07 February 2021)

Abstract–We measured noble gases in "cluster chondrite clasts" from nine unequilibrated ordinary chondrites (UOCs). For five meteorites, we also present data for so-called "clastic matrix," the impact-brecciated material in which the angular to subrounded cluster chondrite clasts are often embedded. Cluster chondrite clasts are characterized by close-fit texture of deformed and indented chondrules with lower amounts of fine-grained interchondrule matrix than in other UOCs (Metzler 2012). They are ubiquitous in UOCs and may indicate accretion and compaction of hot and deformable chondrules within hours or days after formation. Clastic matrix of four of the five meteorites contains He and Ne implanted by the solar wind (SW), indicating that they are regolith breccias. In contrast, cluster chondrite clasts are essentially devoid of SW, confirming that they are fragments of "primary accretionary rocks" (Metzler 2012). Trapped Kr and Xe in all samples are essentially primordial (type "Q"). Trapped Xe concentrations in cluster chondrite clasts are similar to values in other UOCs of similar metamorphic grade despite their low fractions of primordial gas-bearing fine-grained materials. This possibly indicates that the interchondrule matrix in cluster chondrite clasts is more pristine than matrix of regular UOCs. Later loss of primordial gases during parent body metamorphism is mirrored in the decreasing concentrations of primordial noble gases with increasing petrologic type. Relative to cluster chondrite lithologies, clastic matrix often contains excesses of cosmogenic noble gases, most likely due to precompaction exposure in the parent body regolith.

INTRODUCTION

Unequilibrated ordinary chondrites (UOCs) suffered only mild thermal metamorphism on their parent asteroids and hence are carriers of information about early processes in the solar system. However, most of these rocks were affected by impact processes, which transformed formerly coherent material into breccias, consisting of chondritic lithic clasts, embedded in a finer-grained clastic matrix (see, e.g., Scott and Taylor [1982]; Scott [1984]; Bischoff et al. [2006] and references therein). Chondrules in unbrecciated UOCs and in lithic clasts from brecciated UOCs are usually almost spherical and embedded in a fine-grained interchondrule matrix which typically makes up 10–15 vol% of the meteorite (e.g., Weisberg et al. 2006). However, a large fraction of brecciated UOCs also contains clasts characterized by close-fit textures of deformed and indented chondrules (Metzler 2012). Such "cluster chondrite" clasts occur in about 40% of the UOCs studied by Metzler (2012), with clast sizes between <1 mm and ≥10 cm. An example for a cluster chondrite clast in the LL3 chondrite NWA 4522 is shown in Fig. 1. These clasts have the highest chondrule abundances (82–92 vol%) of all chondrite classes and only between 3 and 9 vol% of interchondrule matrix (Metzler 2012). Metzler (2012) proposed that cluster chondrites formed by co-accretion of hot and deformable chondrules together with rigid chondrules and a small fraction of fine-grained matrix. Many chondrules deformed extensively during this process. According to Metzler (2012), this material either formed

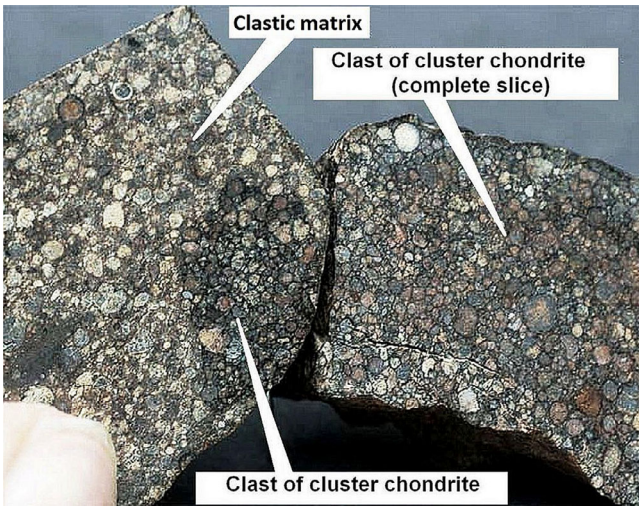

Fig. 1. Texture of the brecciated LL3 chondrite NWA 4522, which consists of subrounded cluster chondrite clasts, embedded in a clastic matrix. This matrix consists mainly of small cluster chondrite clasts, intact chondrules, chondrule fragments, and very fine-grained dust. Courtesy Carsten Giessler; width of image: ~4.5 cm. (Color figure can be viewed at wileyonlinelibrary.com.)

a larger body or reached the surface of an existing body within hours to days after chondrule formation. Later, the resulting rocks ("cluster chondrites") became fragmented by impacts. The resulting rock fragments ("cluster chondrite clasts") were mixed with various other types of chondritic rock fragments, as well as isolated spheroidal chondrules and chondrule fragments. After consolidation (impact compaction) of this smörgåsbord of different materials, the resulting impact breccias now consist of macroscopically detectable cluster chondrite clasts embedded in a finer grained groundmass, that is, the clastic matrix portions. Note that in this paper for simplicity, clastic matrix will mostly just be called "matrix"/"mx." This relation (angular clasts embedded in a clastic matrix) is typical of all kinds of extraterrestrial impact breccias (see Bischoff et al. 2006). According to Metzler (2012) and Metzler and Pack (2016), the cluster chondrite clasts are relicts of primary accretionary rocks and document a process where chondrule-forming heating events and the accretion of chondritic bodies were obviously closely linked in space and time.

Noble gases provide important information about the origin and later history of meteorites and their parent bodies. Noble gases produced by cosmic rays not only allow us to study the exposure history during transfer of a meteorite from its parent body to Earth (e.g., Herzog and Caffee 2014) but in some cases also the history of different constituents of a meteorite near the surface of its parent body (e.g., Wieler et al. 1989) or perhaps even prior to a meteorite's final accretion (e.g., Kööp et al. 2018). The multitude of trapped noble gas components in meteorites allows one to study processes ranging from the presolar epoch until late parent body processes or even the terrestrial history of a meteorite (Wieler et al. 2006; Ott 2014). Ott (2014) provides a detailed review of the noble gas component structure of meteorites. For the purpose of this study, it is sufficient to distinguish between trapped noble gases implanted by the solar wind (SW) and trapped "primordial" noble gases. The former were implanted into the uppermost few nanometers of grains on the surface of a parent body, before these grains became incorporated and compacted into a regolith breccia at a time usually very difficult to constrain (e.g., Wieler et al. 1989). SW noble gases occur in the fine-grained material of many meteorites (Schultz and Franke 2004; Bischoff et al. 2018), testifying of the efficiency of regolith mixing. The most important primordial noble gas component for this paper resides in an ill-characterized carrier known by the acronyms "Q" or "P1," but we will also consider to some extent primordial noble gases known to reside in presolar grains (cf. Ott [2014] and references therein). SW gases reside only in the fine-grained clastic matrix of chondrites. Primordial noble gases occur in the clastic matrix and are also present in the fine-grained material of cluster chondrite clasts (interchondrule matrix). On the contrary, chondrules in UOCs are devoid of both SW and primordial noble gases (Vogel et al. 2004). Compared to the SW noble gases, relative elemental abundances of the primordial components are depleted in the light noble gases He and Ne by many orders of magnitude. For instance, the Q component has an Ne/Xe ratio even lower than that of the major presolar components (Ott 2014). As we will see, the consequence of this is that we will be able to consider the trapped Kr and Xe in our samples as being predominantly Q, whereas the trapped He and Ne —where present in sizeable quantities—will be dominated by the SW component. Trapped He and Ne will thus mainly tell us whether a sample contains fine-grained material from an asteroidal regolith. Primordial Kr and Xe allow us to study potential differences between matrix and cluster chondrite clasts as well as possible gas loss during the accretionary phase or later on the parent body by thermal and/or impact metamorphism (Busemann et al. 2000; Bekaert et al. 2019).

The aim of this work is therefore to shed further light on the formation and evolution of UOCs containing cluster chondrite clasts based on their noble gas records. In the following, it is important to keep in mind the petrologic and genetic differences between "clastic matrix" (here called "matrix") and "interchondrule matrix." We use the term

"interchondrule matrix" only to denote the fine-grained portions interstitial to chondrules in cluster chondrite clasts (see fig. 2B in Metzler and Pack 2016). Interchondrule matrix consists nearly exclusively of μm-sized grains (silicates, sulfides, Fe-Ni metal), which probably represents primitive dust that co-accreted with the chondrules in a single-step accretion event. It represents the main carrier of primordial noble gases in unbrecciated chondritic rocks (e.g., Vogel et al. 2003). We did not measure interchondrule matrix separately in the present study, but it contributes to the noble gas inventory of the analyzed cluster chondrite clasts. The interchondrule matrix is distinct from the clastic matrix, the fine-grained material interstitial to chondrules, and fragments in brecciated UOCs. This material represents debris formed by impact comminution of various chondritic lithologies (see fig. 4 in Metzler 2012). Normally, it represents a mixture of small chondrite fragments of various petrologic types (including cluster chondrites); isolated chondrules and chondrule fragments; as well as certain portions of fine-grained, impact-induced dust. The components of the clastic matrix were affected by mechanical and thermal stress during impact comminution, which may have led to partial degassing of this material. The fine-grained portion of the clastic matrix is usually the sole carrier of SW noble gases. These gases were incorporated into loose mineral grains at the asteroid's very surface by solar irradiation. Regolith gardening transported these grains with their SW load to larger depths (e.g., Wieler et al. 1989; Nakamura et al. 1999; Welten et al. 2011).

The sample suite includes Northwest Africa 869 (NWA 869), the largest known chondritic regolith breccia with about seven tons of recovered material (Metzler et al. 2011). NWA 869 is one of the few L chondritic regolith breccias. This meteorite is therefore of particular interest to study accretionary processes (Hyde et al. 2020).

SAMPLES AND METHODS

Table 1 gives an overview of the samples analyzed from eight LL chondrites and one L chondrite. Five meteorites (NWA 869, NWA 2336, NWA 3119, NWA 4522, NWA 5205) are definitely impact breccias, consisting of cluster chondrite clasts and a finer grained clastic matrix. Samples NWA 5421 and NWA 6742 consist entirely of the cluster chondrite textures, but they almost certainly represent isolated clasts from the paired NWA 5205 breccia. This conclusion is based on the similar texture, chemical and oxygen isotopic composition (Metzler and Pack 2016), and noble gas concentrations (see the Results section). Samples NWA 5206 and NWA 6007 only contain the cluster chondrite texture and are not paired with known samples containing also clastic matrix. Either the latter is missing due to small sample size or the entire meteorites have been blasted out of large-scale coherent rocks on the asteroid and were never part of an impact breccia.

Compared to the official classifications given in the Meteoritical Bulletin Database (MBDB), several samples were reclassified during this investigation. NWA 2336 represents a brecciated LL3, not H3.10, chondrite. This conclusion, based on the variation of olivine composition ($Fa_{27.9\pm8.3}$; $n = 31$) and mean apparent chondrule size (604 μm; $n = 84$), is also supported by oxygen isotope measurements (see MBDB). NWA 3119 is a brecciated LL3, not LL4, chondrite, based on the chemical variability of olivine ($Fa_{26.7\pm8.5}$; $n = 20$). NWA 5205 (and the paired NWA 5421 and NWA 6742, see below) are of petrologic type 3.7, not 3.2 (Metzler 2012; Metzler and Pack 2016). NWA 6007 has to be reclassified from L3 to LL3, based on its mean apparent chondrule size (617 μm; $n = 160$).

The investigated LL chondrites have petrologic subtypes between 3.05 and 3.7, indicating a range of parent body metamorphism. Petrologic types of the investigated cluster chondrite clasts are also listed in Table 1 (determined for this work by K. Metzler). Cluster chondrite clast samples were analyzed from all nine meteorites, and for five of them, matrix samples were also available. Samples for noble gas analyses consisted of sub-mm-sized fragments mixed with finer dust. Sample masses ranged between about 9 and 80 mg, that is, comprising material between tens to several hundred chondrules. Table 1 also lists the fractions of interchondrule fine-grained materials for the cluster chondrite clast samples, estimated from thin sections.

The previously best studied meteorite in our sample suite is NWA 5205, a coarse-grained breccia consisting of huge cluster chondrite clasts (up to ~10 cm), embedded in matrix (Metzler 2012; Metzler and Pack 2016; Metzler et al. 2019). The mean chondrule sizes vary dramatically between different clasts, indicating chondrule size sorting prior to accretion (Metzler et al. 2019). The clasts designated F6d,e,I and PM-A (Table 1) correspond to clasts #1 and #2, respectively, in Metzler (2012), Metzler and Pack (2016), and Metzler et al. (2019).

Another well-studied sample is the L3-6 regolith breccia NWA 869. Two cluster chondrite clasts from this breccia have been studied (Table 1). One of these is of petrologic subtype <3.5 while the other is of type 4, representing the most intensively metamorphosed sample among all studied lithologies. The NWA 869 meteorite belongs to the few (3%) L chondrites containing solar noble gases (Osawa and Nagao 2006;

Table 1. Sample overview.

Meteorite	Classification	Find mass (kg)	Subsample code	Lithology	Petrol. type	Mass (mg)	Fine-grained materials (vol%)
NWA 869[b,c]	L3-6	≥7000	M-06-44-1-a1	ccc	<3.5	79.4	3/5
			M-06-44-1-a2			52.2	
			MS-04-1-b	ccc	4	20.8	–/9*
						40.5*	
			MS-04-1	mx		8.8	
						37.2*	
NWA 2336	LL3	0.402	DFG-B	ccc	3.7	23.4	
			DFG-B	mx		22.1	
NWA 3119[c]	LL3	1.073	DFG-1	ccc	3.5	12.3	12/7
						17.7*	
			DFG	mx		9.3	
						17.9*	
NWA 4522[c]	LL3	0.949	DFG-D-3	ccc	3.5	12.4	13/8
						17.7*	
			DFG-D-5	mx		23.2	
						23.9*	
NWA 5205[c-e]	LL3.7	4.000	#1 (F6 d,e,i)	ccc	3.7	38.4	4/5
						46.4*	
			#2 (PM-A-1)	ccc	3.7	7.6	4/12
						69.2*	
			F-1	mx		17.5	
						47.4*	
NWA 5206[d]	LL3.05	0.126		ccc	<3.5	28.9	5/8
						41.6*	
NWA 5421[d]	LL3.7	2.200		ccc	3.7	19.6	5/9
						35.8*	
NWA 6007	LL3	0.410		ccc	<3.5	49.6	5/5
NWA 6742	LL3.7	0.149	DFG-F	ccc	3.7	21.9	7/4
						26.1*	

Lithologies: "ccc" = cluster chondrite clast; "mx" = matrix/clastic matrix. Petrologic types refer to analyzed cluster chondrite clasts. Asterisk in column "mass" indicates initial analysis (Huber et al. 2013) of the same cluster chondrite clast or matrix sample listed in the row above. Only He, Ne, and ^{36,38}Ar data are given for these samples.

[a]Vol% of interchondrule matrix/metal sulfide in cluster chondrite clasts.

Petrological and chemical descriptions of samples given in: [b]Metzler et al. (2011), [c]Metzler and Pack (2016), [d]Metzler (2012), [e]Metzler et al. (2019). Meteorite classifications of chemical groups and petrologic types done by K. Metzler disagree in several cases with those listed in the Meteoritical Bulletin Database, see the Samples and Methods section.

NWA 5205, NWA 5421, and NWA 6742 are very likely paired; NWA 3119 and NWA 4522 are likely paired (see text).

*Matrix fraction not to be determined due to thermal overprint (recrystallization).

Welten et al. 2011). Also, NWA 869 does not show the young U-Th-He and K-Ar ages typical for many L-chondrites (Metzler et al. 2011), which indicate a late breakup of the L-chondrite parent body ~470 Ma ago (Korochantseva et al. 2007).

Samples were analyzed at ETH Zurich according to procedures given by Riebe et al. (2017b). Briefly, samples wrapped in Al-foil were pre-degassed in the sample holder carousel pumped to ultra-high vacuum for about 24 h at ~120 °C to eliminate adsorbed atmospheric gases. Noble gas extraction was performed in a single heating step at ~1700 °C in a molybdenum crucible. After cleaning, gases were split into three fractions (He&Ne, Ar, Kr&Xe), which were analyzed separately in noncommercial static noble gas mass spectrometers (Riebe et al. 2017b). Occasional re-extractions at slightly higher temperatures all yielded signals comparable to those of blank analyses. Blank measurements were performed by analyzing pieces of Al foils with masses comparable to those used to wrap samples. Blank corrections on the major isotopes of each element typically were on the order of a few percent or below. Occasional blank corrections of up to some 10% (likely caused by a previous analysis of a very gas-rich meteorite sample not related to this project) did in no way compromise the interpretation of the results presented here. Calibrations of the sensitivity and mass discrimination of the mass spectrometer were

done with regular analyses of pure standard noble gases (Heber et al. 2009; Riebe et al. 2017b).

Stated uncertainties of measured concentrations and isotopic ratios (1σ) include ion counting statistics, blank corrections, mass discrimination, and spectrometer sensitivity variations. Uncertainties of calibrations gases (2% for He, Ne, and Ar; 5% for Kr and Xe; Heber et al. 2009) are not included, as they do not affect, for example, exposure age comparisons of different samples studied here.

All noble gas data reported here are available at the ETH repository: https://doi.org/10.3929/ethz-b-000467535

RESULTS

Tables 2 and 3 present the concentrations and isotopic ratios of He, Ne, and Ar as well as the concentrations of ^{84}Kr and ^{132}Xe of the samples analyzed. For many samples, an initial analysis was carried out (Huber et al. 2013), for which only He, Ne, and ^{36,38}Ar are given due to sizeable contamination by atmospheric ^{40}Ar, Kr, and Xe. The isotopic compositions of Kr and Xe are given in Tables A1 and A2 in the Appendix. Table 4 presents the cosmogenic (cos) fractions of ^{3}He, ^{21}Ne, and ^{38}Ar and the resulting cosmic ray exposure ages. Table 5 lists the concentrations of the trapped component of the major isotope of each noble gas, to the extent these could be determined reliably. Table A3 lists the concentrations of radiogenic ^{4}He, ^{40}Ar, and ^{129}Xe (^{129}Xe*).

The numbers in Tables 4, 5, and A3 are calculated as follows: For cosmogenic ^{3}He, we assumed that samples with $^{4}He < 1000 \times 10^{-8}$ cm^{3}STP per g do not contain any trapped (tr) He, hence, $^{3}He_{cos} = {}^{3}He_{meas}$. For the other samples, $^{3}He_{meas}$ was corrected for trapped He of assumed SW composition ($^{3}He/^{4}He = 4.64 \times 10^{-4}$; Heber et al. 2009). The SW ^{4}He concentration was calculated by correcting measured ^{4}He for an assumed radiogenic contribution of 800×10^{-8} cm^{3}STP per g and cosmogenic ^{4}He via $(^{4}He/^{3}He)_{cos} = 6.1$ (Alexeev 1998). Cosmogenic ^{21}Ne was calculated with a two-component deconvolution of trapped and cosmogenic Ne. Trapped Ne was assumed to be either Ne-Q (Ott 2014) or fractionated SW-Ne, depending on, for example, the ^{4}He concentration of a given sample (samples with $^{4}He > 1000 \times 10^{-8}$cm^{3}STP per g are assumed to contain SW-Ne, as confirmed by the Ne isotopic composition; the SW-bearing samples are marked with "*" in Table 2). For samples with little trapped Ne $(^{20}Ne/^{21}Ne)_{meas} < 2.6$, the $(^{22}Ne/^{21}Ne)_{cos}$ ratios are also given in Table 4. They were determined assuming the respective $(^{20}Ne/^{22}Ne)_{tr}$ ratio (Q or SW). Cosmogenic ^{38}Ar was calculated by a two-component deconvolution of trapped and cosmogenic Ar, with $(^{36}Ar/^{38}Ar)_{cos} = 0.65$ and $(^{36}Ar/^{38}Ar)_{tr} = 5.34$ (Ar-Q; Busemann et al. 2000), or, in the few cases where the presence of SW gases is evident (marked by stars in Table 2), with $(^{36}Ar/^{38}Ar)_{tr} = 5.48$ (Heber et al. 2009). Trapped ^{84}Kr and ^{132}Xe are almost identical to measured values, with slight corrections for cosmogenic contributions. These were based on two-component deconvolutions involving ^{78}Kr and ^{126}Xe concentrations, trapped Kr and Xe isotopic compositions for the Q-component (Busemann et al. 2000), and cosmogenic $^{78}Kr/^{84}Kr$ and $^{126}Xe/^{132}Xe$ ratios (Wieler 2002a, "chondrites" and "meteorites"). Table A3 lists the radiogenic ^{4}He concentration for those samples for which it can be estimated with some confidence (correcting for $^{4}He_{cos}$ with $[^{4}He/^{3}He]_{cos} = 6.1$ and assuming no trapped ^{4}He). Especially the very low numbers $< 31 \times 10^{-8}$cm^{3}STP per g should be viewed as upper limits, since minor amounts of trapped ^{4}He will also be present. Radiogenic ^{40}Ar is assumed in all cases to be equal to the measured ^{40}Ar values. Radiogenic ^{129}Xe* is calculated by correcting for trapped Xe-Q, using $^{131\text{-}136}$Xe corrected very slightly for cosmogenic contributions.

Before we present the data in detail, we summarize its main features:

1. With one exception, matrix samples contain sizeable amounts of trapped noble gases, predominantly implanted SW, which governs the He and Ne isotopic and elemental abundance patterns.
2. The cluster chondrite clast samples are devoid of SW He and Ne (except for one sample of NWA 869 contaminated with fine-grained material from adjacent matrix).
3. All samples contain trapped Ar, Kr, and Xe dominated by the primordial Q-component, as evidenced by their isotopic and elemental compositions. The primordial gases must reside essentially in the fine-grained portions of the clast and matrix samples. Concentrations of trapped Kr and Xe tend to decrease with increasing petrologic type of the host meteorite, as is generally observed in UOCs (Anders and Zadnik 1985). Trapped Xe concentrations of cluster chondrite clasts are similar to values of other UOCs of corresponding types.
4. All samples contain cosmic ray–produced noble gases. Matrix samples often contain higher concentrations of cosmogenic noble gases than cluster chondrite clasts from the same meteorite. This is most likely due to a precompaction exposure of matrix material in the parent body regolith that probably occurred simultaneously with implantation of SW noble gases.
5. The three meteorites NWA 5205, NWA 5421, and NWA 6742 have similar cosmic ray exposure ages

Table 2. He and Ne concentrations and isotopic compositions.

	Lithol.	^{3}He	±	^{4}He	±	^{20}Ne	±	^{20}Ne/^{22}Ne	±	^{21}Ne/^{22}Ne	±
NWA 869	ccc a1*	0.488	0.003	751	4	11.51	0.24	10.30	0.02	0.1770	0.0006
	ccc a2*	0.531	0.004	1210	5	73.1	3.5	12.99	0.62	0.06697	0.00028
	ccc b	8.03	0.05	854	5	2.422	0.019	0.858	0.004	0.9316	0.0026
		7.32	0.20	1099	24	2.08	0.08	0.858	0.017	0.925	0.004
	mx*	9.80	0.09	2547	20	375	8	10.66	0.02	0.1438	0.0003
	*	10.0	0.3	4037	90	351	6	10.7	0.4	0.1453	0.0009
NWA 2336	ccc	10.4	0.1	865	15	2.200	0.018	0.961	0.004	0.831	0.003
	mx*	10.2	0.1	1105	20	41.5	1.2	7.12	0.21	0.3862	0.0014
NWA 3119	ccc	30.8	0.2	866	5	8.65	0.07	0.946	0.004	0.9035	0.0022
		31.7	0.9	1288	29	8.77	0.26	0.948	0.011	0.901	0.003
	mx*	68.4	0.4	74020	410	544	7	9.46	0.12	0.1902	0.0007
	*	79.2	2.2	112000	2500	673	21	9.98	0.11	0.1809	0.0019
NWA 4522	ccc	27.3	0.3	2749	43	20.47	0.20	2.082	0.010	0.8001	0.0023
		27.9	0.8	3586	80	19.9	0.60	1.985	0.013	0.799	0.004
	mx*	78.5	1.1	161100	650	696	11	9.86	0.11	0.1443	0.0013
	*	98.0	2.7	181000	4000	822	13	8.86	0.30	0.1331	0.0004
NWA 5205	ccc F	1.84	0.01	17.7	0.4	1.33	0.04	1.09	0.03	0.8921	0.0026
		1.78	0.01	n.d.		1.388	0.008	1.216	0.005	0.880	0.003
	ccc P	1.51	0.02	39.9	2.6	1.48	0.03	1.365	0.026	0.851	0.005
		1.62	0.05	38.9	0.9	1.60	0.05	1.443	0.024	0.848	0.005
	mx	1.76	0.01	34.5	0.9	1.63	0.09	1.44	0.08	0.857	0.004
		1.74	0.05	34.8	1.0	1.60	0.06	1.50	0.03	0.862	0.006
NWA 5206	ccc	21.4	0.2	942	4	9.15	0.17	1.248	0.006	0.8792	0.0021
	ccc	21.0	0.2	874	13	7.98	0.20	1.113	0.005	0.8948	0.0024
NWA 5421	ccc	1.77	0.02	22.0	0.6	1.246	0.012	1.201	0.007	0.889	0.004
		0.841	0.084	34.0	1.0	1.33	0.04	1.281	0.008	0.857	0.004
NWA 6007	ccc	18.0	0.1	966	19	5.75	0.04	1.144	0.004	0.8592	0.0015
NWA 6742	ccc	1.78	0.02	17.6	0.7	1.548	0.014	1.327	0.009	0.874	0.003
		1.66	0.05	34.8	1.0	1.69	0.05	1.643	0.015	0.836	0.006

Gas concentrations in [10^{-8} cm^{3}STP per g]. Uncertainties (1σ) include ion counting statistics, mass discrimination, and spectrometer sensitivity variations. Uncertainties of calibrations gases (2%, Heber et al. 2009) not included.

Samples unequivocally containing SW-implanted Ne (and likely He & Ar) marked by asterisk in column "Lithol." For "ccc" and "mx," see Table 1.

and similar—exceptionally low—concentrations of radiogenic ^{4}He and ^{40}Ar, respectively, indicating that these meteorites are paired. This conclusion is strongly supported by their very similar chemical and petrographic characteristics. Additionally, the samples NWA 3119 and NWA 4522 share many similarities in their noble gas signatures, which also indicate pairing. Again, this conclusion is strongly supported by petrographic observations.

Trapped He, Ne (and Ar) Implanted by the SW in Matrix Samples

The implanted SW noble gas component in the matrix samples is best visualized in the Ne three-isotope diagram in Fig. 2. Except for NWA 5205, the data points of all matrix samples plot toward the trapped components in the upper left corner. These data points mostly indicate a trapped ^{20}Ne/^{22}Ne ratio of 11−12.5, that is, in the range of fractionated SW (Grimberg et al. 2006), as expected for implanted SW-Ne in lunar and meteoritic samples (e.g., Wieler 2016). The initial analysis of the matrix sample of NWA 4522 shows a lower $(^{20}Ne/^{22}Ne)_{tr}$ ratio of only ~10. This indicates some atmospheric Ne contamination, possibly due to insufficient pre-degassing. Concentrations of $^{20}Ne_{tr}$ (Table 5) of all matrix samples are much higher than values to be expected for primordial Ne in UOCs of petrologic types 3.5 or higher (e.g., Schultz and Franke 2004), confirming an SW origin of the overwhelming fraction of the trapped Ne even in the samples with the lowest $(^{20}Ne/^{22}Ne)_{tr}$ ratios. The two meteorites with the highest ^{4}He concentrations, for which a reasonably accurate correction for cosmogenic, radiogenic, and primordial ^{4}He is possible (NWA 3119 and NWA 4522), have $(^{4}He/^{20}Ne)_{tr}$ values of 150–170, typical for fractionated SW in meteorite samples (Wieler et al. 1989; Wieler 2002b). The two matrix samples of NWA

Table 3. Ar, Kr, and Xe concentrations and $^{36}Ar/^{38}Ar$.

	Lithol.	^{36}Ar	±	^{40}Ar	±	$^{36}Ar/^{38}Ar$	±	^{84}Kr	±	^{132}Xe	±
NWA 869	ccc a1	19.8	0.2	6005	75	5.37	0.03	10.0	0.5	7.6	1.1
	ccc a2	18.4	0.2	4310	55	5.25	0.03	10.3	0.3	10.5	0.3
	ccc b	2.11	0.11	5560	450	4.02	0.30	2.34	0.14	2.75	0.41
		2.57	0.02			4.16	0.18				
	mx	13.8	0.3	3920	120	4.85	0.13	2.42	0.19	2.0	0.3
		13.5	0.1			4.91	0.04				
NWA 2336	ccc	9.94	0.29	2640	110	4.98	0.13	8.75	0.11	8.02	0.19
	mx	12.4	0.1	2465	130	4.80	0.10	9.38	0.11	8.31	0.19
NWA 3119	ccc	49.8	0.3	1675	20	5.07	0.03	26.8	1.4	19.2	2.9
		49.0	0.2			5.00	0.02				
	mx	43.0	0.3	4505	40	4.84	0.02	13.9	0.7	9.0	1.3
		49.1	0.2			4.87	0.02				
NWA 4522	ccc	42.5	0.3	5805	65	4.85	0.03	43.3	2.3	30	4
		45.5	0.2			5.01	0.02				
	mx	50.7	0.9	4365	110	4.90	0.04	12.1	0.7	8.6	1.3
		57.2	0.3			4.91	0.02				
NWA 5205	ccc F	5.16	0.17	106	5	4.65	0.11	6.21	0.13	6.11	0.13
		6.84	0.09			4.41	0.10				
	ccc P	12.7	0.9	461	46	4.94	0.05	16.5	0.3	10.7	0.3
		9.21	0.04			4.85	0.04				
	mx	19.2	0.7	180	10	5.26	0.15	17.6	0.3	16.4	0.4
		16.2	0.1			5.06	0.05				
NWA 5206	ccc	113.4	0.6	2585	20	5.23	0.02	66	3	45	7
	ccc	91.2	0.7			5.58	0.20				
NWA 5421	ccc	7.13	0.13	185	7	4.77	0.12	12.0	0.6	8.4	1.2
		10.1	0.1			4.93	0.03				
NWA 6007	ccc	36.7	1.0	4855	190	5.25	0.42	42.3	0.6	41.2	1.0
NWA 6742	ccc	14.0	0.2	185	3	4.81	0.07	11.2	0.5	10.4	1.2
		18.0	0.1			5.16	0.02				

Gas concentrations in [10^{-8} cm^3STP per g] for $^{36,40}Ar$ and in [10^{-10} cm^3STP per g] for ^{84}Kr and ^{132}Xe. Uncertainties (1σ) include ion counting statistics, mass discrimination and spectrometer sensitivity variations. Uncertainties of calibrations gases (2% for Ar, 5% for Kr and Xe; Heber et al. 2009) not included. Isotopic ratios of Kr and Xe given in Tables A1 and A2. For "ccc" and "mx," see Table 1.

869 show an exceptionally fractionated SW component. Welten et al. (2011) already observed this, reporting an average $^4He/^{20}Ne$ value of only ~7.3. Our average value of 6.9 ± 2.1 is similar to this value (obtained using the correlation between non-cosmogenic ^4He and trapped ^{20}Ne, cf. Welten et al. 2011). These authors argue that most of the SW-He loss in NWA 869 occurred during thermal events on the L chondrite parent body before compaction of the future meteorite.

Trapped He, Ne (and Ar) in Cluster Chondrite Clast Samples

In contrast to the matrix samples, cluster chondrite clast (ccc) samples from only one of the nine meteorites studied (subsample M-06-44-1-a; ccc a from NWA 869) contain variable amounts of trapped Ne with an SW-like isotopic signature. Concentrations of trapped Ne in the two analyzed aliquots differ by a factor of ~7 (Table 5), indicating an admixture of different amounts of matrix material adhering to these samples as a result of the irregular outline of this clast. Two analyses of a second cluster chondrite clast (MS-04-1-b; ccc b) from the same meteorite do not show an SW signature. The inference that the SW-Ne in ccc a is due to contamination by matrix material is strongly supported by sample ccc a2, for which a rough correction for radiogenic ^4He can be made. This sample shows an exceptionally low ratio of trapped $^4He/^{20}Ne$ of about 6 (Table 5), close to the values of the two matrix samples of NWA 869. The Ne data points of all other cluster chondrite clast samples fall near the cosmogenic endmember in the lower right corner of Fig. 2. The isotopic composition of the minor amounts of trapped Ne in these samples cannot be determined with reasonable accuracy. In some cases, it will be essentially purely primordial Ne (a mixture of Q and presolar gases). However, in NWA 4522 and possibly also in NWA 3119, a minor contamination of the cluster chondrite clasts with SW-bearing matrix material seems

Table 4. Cosmogenic noble gases and exposure ages.

	Lithol.	$^{3}He_{cos}$	±	$^{21}Ne_{cos}$	±	$^{38}Ar_{cos}$	±	$(^{22}Ne/^{21}Ne)_{cos}$	T3	**T21**	T38
NWA 869	ccc a1	0.488	0.003	0.170	0.003				0.4[b]	**0.5**[b]	
	ccc a2	0.345	0.004	0.195	0.007				0.3[b]	**0.6**[b]	
	ccc b	8.03	0.05	2.63	0.02	0.15	0.05	1.071	5.0	**6.0**	2.8
		7.2	0.2	2.24	0.08	0.16	0.03	1.079	4.6	**5.3**	3.1
	mx	9.0	0.1	4.15	0.09	0.30	0.09		5.8	**9.6**	5.9
		8.6	0.3	3.93	0.07	0.25	0.02		5.4	**9.1**	5.0
NWA 2336	ccc	10.4	0.1	1.90	0.02	0.16	0.06	1.191	6.9	**9.0**	4.3
	mx	10.1	0.1	2.15	0.06	0.30	0.06		6.7	**10**	8.2
NWA 3119	ccc	30.8	0.2	8.26	0.07	0.58	0.06	1.096	16	**21**	12
		31.5	0.9	8.33	0.25	0.73	0.04	1.099	17	**21**	16
	mx	35[a]	3	9.62	0.13	0.97	0.05		18[a]	**24**	21
		29[a]	5	10.6	0.4	1.04	0.04		15[a]	**27**	22
NWA 4522	ccc	26.5	0.3	7.83	0.08	0.93	0.06	1.120	15	**23**	22
		26.7	0.8	7.99	0.24	0.65	0.04	1.131	15	**25**	16
	mx	5[a]	5	8.16	0.14	0.99	0.09		2.9[a]	**25**	24
		16[a]	8	9.99	0.17	1.08	0.06		8.8[a]	**31**	26
NWA 5205	ccc F	1.84	0.09	1.08	0.03	0.17	0.03	1.097	0.97	**2.7**	3.5
		1.78	0.09	1.00	0.01	0.31	0.04	1.100	0.94	**2.6**	6.6
	ccc P	1.51	0.09	0.923	0.020	0.23	0.03	1.123	0.79	**2.7**	5.4
		1.62	0.10	0.939	0.032	0.20	0.02	1.119	0.85	**2.7**	4.7
	mx	1.76	0.09	0.963	0.052			1.107	0.92	**2.6**	
		1.74	0.10	0.918	0.034	0.20	0.04	1.097	0.91	**2.3**	4.2
NWA 5206	ccc	21.4	0.2	6.44	0.05			1.098	11	**16**	
		21.0	0.2	6.41	0.05			1.091	11	**16**	
NWA 5421	ccc	1.76	0.09	0.921	0.010	0.19	0.04	1.091	0.93	**2.2**	3.8
		0.84	0.12	0.888	0.030	0.18	0.01	1.123	0.44	**2.6**	4.3
NWA 6007	ccc	17.9	0.1	4.32	0.03			1.134	11	**14**	
NWA 6742	ccc	1.78	0.09	1.02	0.01	0.33	0.05	1.097	0.93	**2.6**	7.1
		1.66	0.10	0.858	0.030			1.115	0.87	**2.4**	

Gas concentrations in (10^{-8} cm^3STP per g), exposure ages T3, T21, T38 in (Ma). Uncertainties (1σ) include ion counting statistics, mass discrimination, and spectrometer sensitivity variations. Uncertainties of calibrations gases (2% for Ar, 5% for Kr and Xe; Heber et al. 2009) not included. Production rates for cosmogenic ^{3}He, ^{21}Ne, and ^{38}Ar used to calculate T3, T21, and T38, respectively, are estimated as explained in text. T21 values are preferred. Uncertainties are mostly ~15–20% for T21 due to imprecisely known chemical compositions of analyzed samples and critical assumptions on sample shielding and likely larger for T3 and T38.

[a]$^{3}He_{cos}$ and T3 ages have high uncertainties due to correction for SW contribution.

[b]Low nominal T3 and T21 values of cluster chondrite clast a of NWA 869 reflect very high shielding of this clast and have no age meaning, see text. For "ccc" and "mx," see Table 1.

likely, as the trapped ^{20}Ne concentrations of the cluster chondrite clast samples of these LL3 chondrites are too high to be explained as purely primordial Ne.

Primordial Q Gases for Ar, Kr, and Xe in All Samples

Xenon three-isotope diagrams (one example is shown in Fig. A1) show that the Xe in cluster chondrite clasts as well as in matrix samples is predominantly a mixture of primordial Q-Xe plus some Xe-HL as well as atmospheric Xe. There is no indication of a sizeable contribution of SW-Xe in any of the samples, including the matrix samples rich in SW-He and SW-Ne. This is no surprise, since with very few exceptions even in the most SW-rich meteorite samples, the primordial Q-Xe still swamps the SW-Xe component (Pedroni and Begemann 1994; Mathew and Marti 2003). In our sample with the highest ratio of $^{20}Ne_{tr}/^{132}Xe_{tr}$ (~16,300; NWA 869 mx#1, Table 5), not more than ~5% of the Xe can be of SW origin, since chondritic regolith breccias have ratios of $^{20}Ne_{SW}/^{132}Xe_{SW}$ on the order of 300,000 (e.g., Wieler et al. 1989; Wieler 2002b). The Kr isotope data are not sufficiently precise to distinguish between SW and Q components, but the elemental ratios ^{84}Kr/^{132}Xe (Table 5) indicate that also trapped Kr is dominated by the Q component rather than the SW component.

Chondrites from hot deserts often contain sizeable amounts of possibly tightly bound atmospheric Kr and Xe (Scherer et al. 1994), which may necessitate care when discussing trapped heavy noble gases. Unfortunately, a precise correction of trapped Xe (and

Table 5. Trapped noble gases.

	Lithol.	$^{4}He_{tr}$	$^{20}Ne_{tr}$	±	$^{36}Ar_{tr}$	±	$^{84}Kr_{tr}$	±	$^{132}Xe_{tr}$	±	4/20	20/36	36/84	84/132
NWA 869	ccc a1*		10.0	1.5	19.8	0.2	9.74	0.55	7.61	1.1		0.51	203	1.28
	ccc a2*	~400	72.8	3.6	18.2	0.2	10.1	0.3	10.5	0.3	~5.5	4.00	180	0.96
	ccc b	260	≤0.3		2.0	0.1	2.29	0.14	2.75	0.4			86	0.83
			≤0.5		2.4	0.1								
	mx*	1690	330	50	13.5	0.3	2.36	0.19	2.02	0.3	5.1	24.3	573	1.17
	*	3180	340	10	13.3	0.1					9.3	25.6		
NWA 2336	ccc		≤0.9		9.8	0.1	8.57	0.12	8.01	0.2			114	1.07
	mx*	250	35	5	12.2	0.1	9.19	0.12	8.31	0.2	7.0	2.89	133	1.11
NWA 3119	ccc		2.1	0.9	49.2	0.3	26.2	1.4	19.2	2.9		0.042	188	1.36
		310	2.3	1.6	48.5	0.3					137	0.047		
	mx*	72,800	490	70	42.2	0.3	13.5	0.7	8.95	1.3	149	11.6	312	1.51
		110,400	660	20	48.2	0.3					168	13.7		
NWA 4522	ccc	1800	13.2	0.7	41.8	0.3	42.3	2.3	30.3	4.5	136	0.32	99	1.39
		2630	15	3	41.7	0.3					178	0.33		
	mx	160,000	670	50	49.9	0.9	11.8	0.7	8.60	1.3	239	13.4	422	1.37
		179,000	940	20	56.3	0.5					192	16.6		
NWA 5205	ccc F		≤0.5		5.0	0.1	6.09	0.14	6.11	0.1			83	1.00
			≤0.6		6.6	0.1								
	ccc P		≤0.8		12.5	0.9	16.2	0.3	10.7	0.3			77	1.50
			≤1.1		9.1	0.1								
	mx		≤0.9		19.1	0.1	17.2	0.3	16.4	0.4			111	1.05
			≤1.0		16.0	0.1								
NWA 5206	ccc		3.0	1	113	0.7	64.6	3.5	45.2	6.7		0.027	175	1.43
	ccc		≤2.2		91	0.7								
NWA 5421	ccc		≤0.5		7.0	0.2	11.7	0.6	8.41	1.2			60	1.39
			≤0.9		9.9	0.1								
NWA 6007	ccc	60	≤2.8		36.1	0.3	41.4	0.6	41.2	1.0			87	1.01
NWA 6742	ccc		≤0.8		13.7	0.2	10.9	0.5	10.4	1.2			126	1.05
			1.0	0.2	17.9	0.1								

Concentrations in (10^{-8} cm^3STP per g) for trapped ^{4}He, ^{20}Ne, and ^{36}Ar and in [10^{-10} cm^3STP per g] for ^{84}Kr and ^{132}Xe. Trapped components calculated as explained in text. If no values are given, concentrations are below detection limit, or—for Kr and Xe in the initial analyses—affected by severe atmospheric contamination. The last four columns represent ratios of concentrations of trapped components of respective isotopes.

Samples unequivocally containing SW-implanted Ne (and likely He & Ar) are marked by asterisks in column "Lithol." For "ccc" and "mx," see Table 1.

Kr) for atmospheric contributions is compromised by the rather large uncertainties of isotopic ratios dictated by the often small sample size. However, Fig. 3 (adapted from Scherer et al. 1994), showing trapped $^{132}Xe_{tr}$ versus trapped $^{84}Kr_{tr}$ (Table 5), allows us to judge the extent of atmospheric contamination. Note that the atmospheric $^{84}Kr/^{132}Xe$ ratio is more than 30 times higher than the value of the meteoritic Q component; hence, the relative contamination by atmospheric Kr will very likely considerably exceed that of atmospheric Xe. All data points in Fig. 3 fall somewhat to the right of the dashed line, which is the best-fit line defined by H3 and H4 chondrite fall data given by Scherer et al. (1994). Most data points also fall somewhat to the right of the dotted line, which represents the $^{84}Kr/^{132}Xe$ ratio of 0.81 of the Q component (Busemann et al. 2000). However, all points fall considerably to the left of the dash-dotted line that shows the trend defined by the majority of the hot desert meteorite finds in Scherer et al. (1994). The figure thus indicates that most of our meteorites indeed contain some atmospheric contamination, perhaps up to roughly 50% for Kr, but very likely considerably less for Xe. However, the figure illustrates that the fraction of atmospheric Kr and—especially—Xe in the meteorites studied here is considerably smaller than in the Scherer et al. data set. One reason for this is that we studied almost exclusively UOCs, which have considerably higher concentrations of trapped noble gases. In the Discussion section, we will largely focus on the concentrations of trapped Xe in our samples, as Xe is least affected by atmospheric and SW contributions.

Also for Ar, the isotopic compositions of the trapped gases are not diagnostic to distinguish between SW and primordial (mostly Q) noble gases, which have a very similar Ar isotopic composition. The measured

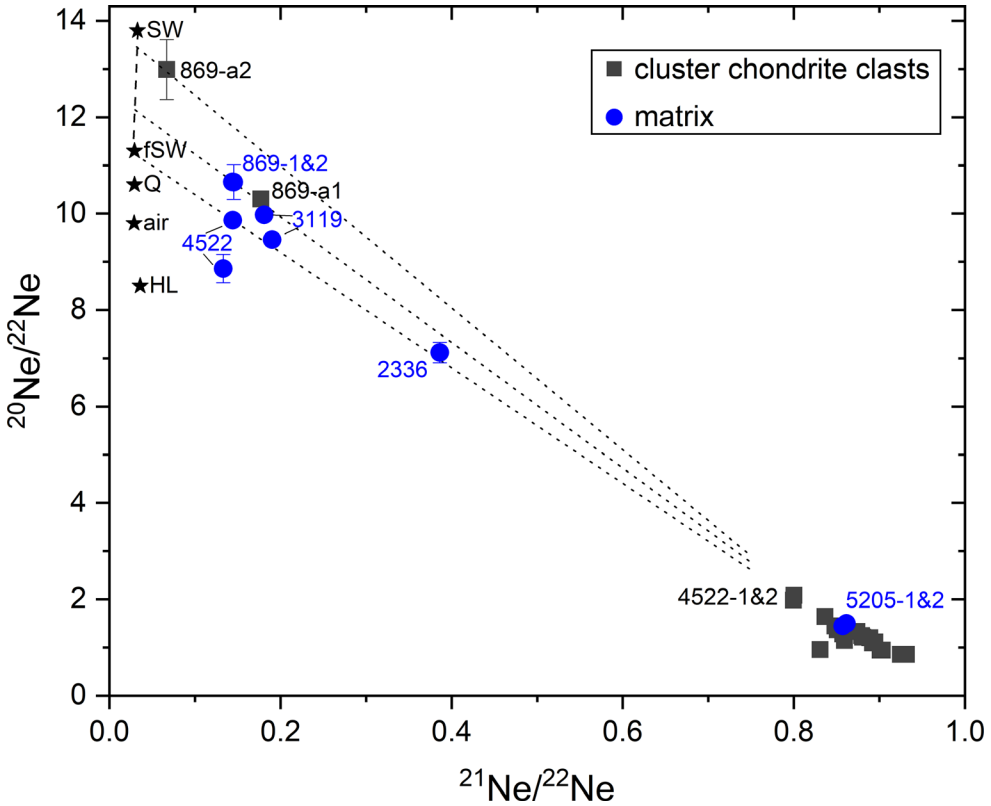

Fig. 2. Ne three-isotope diagram. Labels indicate meteorite name without prefix "NWA." The dashed line in the upper left represents possible compositions of trapped SW (between the pure SW composition and a fractioned "endmember" known as fSW). Q and HL are two trapped components in meteorites (Ott 2014). Except for NWA 5205, all matrix samples contain trapped Ne with $^{20}Ne/^{22}Ne$ ratios close to or higher than fractionated solar wind (fSW), while with one exception, all cluster chondrite clast data points plot near the cosmogenic endmember (the initial analysis of NWA 4522 suffered atmospheric Ne contamination, see the Trapped He, Ne (and Ar) Implanted by the SW in Matrix Samples section). Both subsamples of the exceptional clast NWA 869a indicate contamination with SW-bearing matrix material. $^{20}Ne/^{22}Ne$ ratios of trapped Ne of matrix samples given in Table 5 can be read off the extrapolations of the dotted two-component mixing lines at $^{21}Ne/^{22}Ne \sim 0.03$. (Color figure can be viewed at wileyonlinelibrary.com.)

$^{36}Ar/^{38}Ar$ ratios of all samples are furthermore lowered by cosmogenic Ar. The elemental ratios $^{20}Ne_{tr}/^{36}Ar$ and $^{36}Ar/^{132}Xe$ (Table 5) indicate, however, that the trapped Ar in the samples richest in SW-Ne is a mixture of SW and primordial (Q) Ar.

Cosmogenic Noble Gases

Table 4 shows the concentrations of cosmogenic ^{3}He, ^{21}Ne, and ^{38}Ar in all samples for which these values could be determined with reasonable accuracy. The table also shows the corresponding nominal 4π galactic cosmic ray (GCR) exposure ages, T3, T21, and T38. The production rates of cosmogenic He, Ne, and Ar used to calculate T3, T21, and T38 were determined individually for each meteorite as follows: For every sample of a given meteorite, the same value for the shielding indicator $(^{22}Ne/^{21}Ne)_{cos}$ was adopted as the average value of all samples of this meteorite for which a reliable $(^{22}Ne/^{21}Ne)_{cos}$ ratio could be determined. T21 and T38 were then determined according to David and Leya (2019, equations 6 and 7). T3 was estimated from the depth- and size-dependent production rates of Leya and Masarik (2009). In all cases, these procedures use the $(^{22}Ne/^{21}Ne)_{cos}$ ratio as shielding indicator and assume average chemical composition of the respective meteorite group. For P3, we assumed a meteoroid size of ≤40 cm for all meteorites except NWA 869 (find mass = 7000 kg) for which we adopted a radius of 100 cm. As is often the case, the true shielding of a given sample may be imperfectly constrained by the $(^{22}Ne/^{21}Ne)_{cos}$ ratio; hence, the exposure ages given in Table 4 have substantial uncertainties. For the preferred age, T21, uncertainties are on the order of 15–20%, while they are likely larger for T3 and T38 due to possible gas loss (^{3}He) and variations in the abundances of the major target element Ca (for ^{38}Ar), see the next paragraph. However, as we are mainly interested in

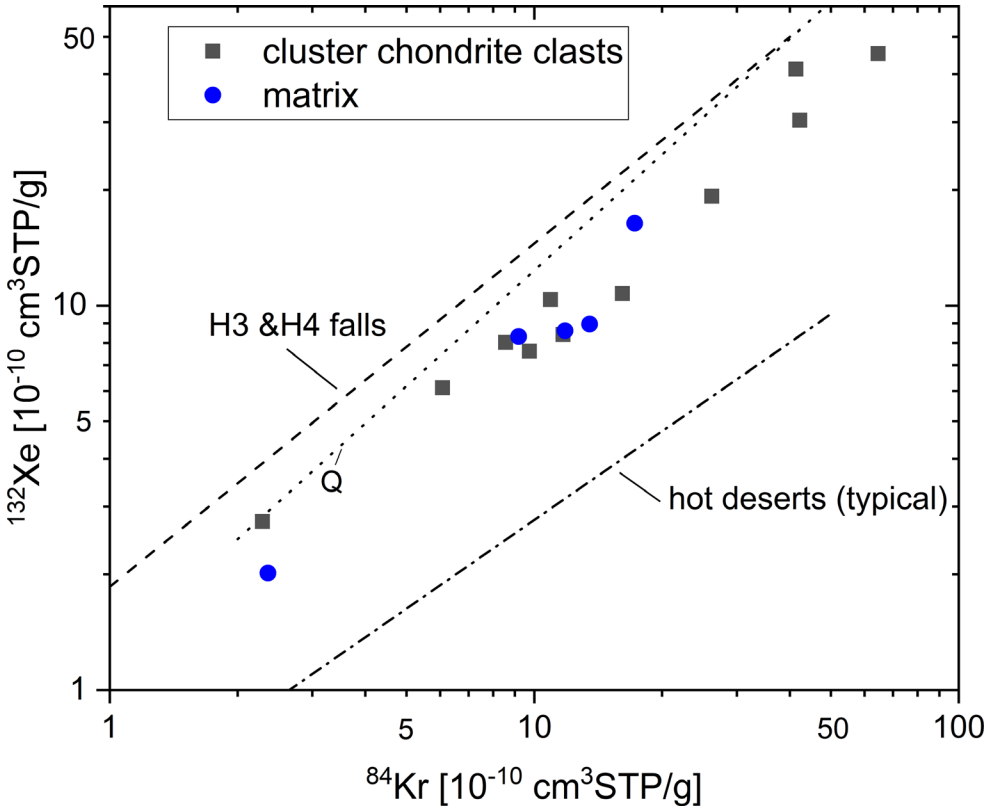

Fig. 3. Trapped ^{132}Xe versus trapped ^{84}Kr of cluster chondrite clast and matrix samples. The dashed line shows the fit line defined by data from H3 and H4 chondrite falls given by Scherer et al. (1994), the dash-dotted line shows a trend defined by the majority of hot desert meteorite finds given by the same authors. The dotted line represents the ^{84}Kr/^{132}Xe ratio of 0.81 for the pure Q component (Ott 2014). All data points plot to the right of both the lines representing H3 and H4 falls and the Q component, indicating some contamination by atmospheric Kr and—less so—Xe. (Color figure can be viewed at wileyonlinelibrary.com.)

possible differences between nominal exposure ages of cluster chondrite clasts and matrix samples of the same meteorite, that is, a possible irradiation by cosmic ray particles prior to the final compaction of a meteorite, uncertainties related to shielding corrections can essentially be neglected. Uncertainties in the effective target element concentrations of each sample will remain a relevant source of uncertainty.

The nominal 4π exposure ages shown in Table 4 and Fig. 4 assume that a sample experienced a single stage of exposure to GCR in a meteoroid of modest size, such that cosmogenic nuclides are produced by particles arriving from the entire 4π space angle. As is often observed in meteorite studies, ^{3}He-based ages (T3) of most of our samples are lower than their respective ^{21}Ne (T21) and ^{38}Ar (T38) ages, suggesting loss of ^{3}He$_{cos}$. Our T38 and T21 also often deviate considerably from each other. This is again often observed and is usually explained by inhomogeneous Ca concentrations in samples of rather low mass (Di Gregorio et al. 2019), which in our cases were mostly below 50 mg and in some cases even below 10 mg. We therefore mainly rely here on the T21, given in bold face in Table 4 and shown in Fig. 4.

The T21 values mostly range between ~2 and ~30 Ma, exposure ages typical for LL- and L chondrites (Herzog and Caffee 2014). Below we identify two sets of meteorites that are possibly or likely paired based on their trapped or radiogenic noble gases. The meteorites in these sets also have similar exposure ages: All samples of the two very SW gas-rich LL chondrites NWA 3119 and NWA 4522 have T21 within 21 and 31 Ma (the highest ages observed here), and the three extremely ^{4}He- and ^{40}Ar-poor LL chondrites NWA 5205, NWA 5421, and NWA 6742 have T21 between 2.2 and 2.7 Ma. Petrographic observations clearly support pairing of these two sample groups: One group (NWA 5205, NWA 5421, NWA 6742) is characterized by an extremely large mean chondrule size, very low amounts of interchondrule matrix, and slightly higher bulk CaO concentrations than typical LL3 chondrites (Metzler 2012; Metzler and Pack 2016). The samples of the other group (NWA 3119, NWA 4522) are characterized by a slightly porous, brownish

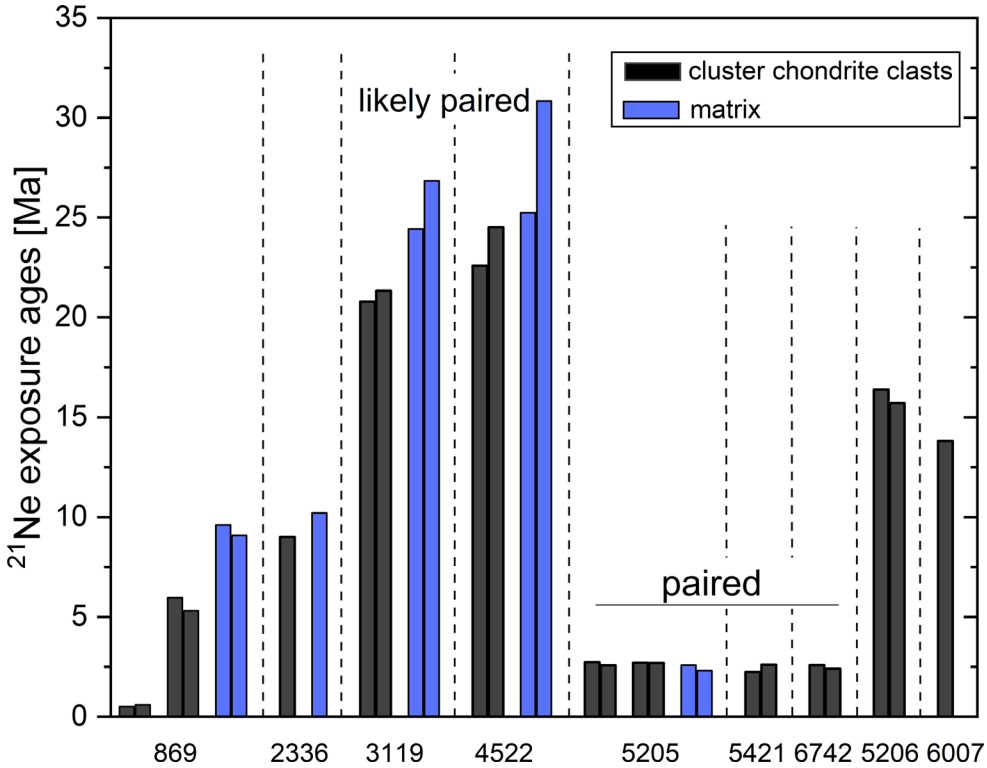

Fig. 4. ^{21}Ne exposure ages (Ma) of all samples analyzed (abscissa labels represent meteorite names without prefix "NWA"). Cluster chondrite clast and matrix samples shown in gray and blue bars, respectively. Adjacent bars indicate two subsamples of the same lithology of the same meteorite (Table 1). Low nominal exposure ages of cluster chondrite clast a of NWA 869 (leftmost two bars) reflect very high shielding of this clast and have no age meaning; see text. Higher nominal exposure ages of matrix samples of NWA 869, NWA 3119, and NWA 4522 relative to respective cluster chondrite clasts indicate pre-exposure in parent body regolith. Similar exposure ages of NWA 5205, NWA 5421, and NWA 6742 on the one hand and of NWA 3119 and NWA 4522 on the other hand are evidence for these meteorites being paired. (Color figure can be viewed at wileyonlinelibrary.com.)

groundmass (clastic matrix) that contains intact chondrules, chondrule fragments, and some impact melt rock clasts. In this groundmass, mm- to cm-sized dark cluster chondrite clasts are embedded (see Fig. 1). Cut faces from both samples are indistinguishable from each other.

A remarkably low nominal exposure age of only 0.5–0.6 Ma is observed for the two analyzed subsamples of NWA 869 of the cluster chondrite clast M-06-44-1-a (Table 4, analyses ccc a1 and ccc a2). This age is much lower than the values between about 5 and 10 Ma of the four other samples of this meteorite analyzed here and also much lower than the 4π exposure age of 5 ± 1 Ma derived by Welten et al. (2011) based on ^{21}Ne and ^{26}Al in many samples of NWA 869. We conclude that this clast has been in the center region of the NWA 869 meteoroid, resulting in a cosmogenic noble gas production rate roughly an order of magnitude below those of other samples from this meteorite. No reliable shielding information is available, as the contamination with SW-Ne inhibits to derive the $(^{22}Ne/^{21}Ne)_{cos}$ ratio (the nominal ages given in Table 4 are based on an assumed value of 1.11 often used for "average" shielding conditions). According to model calculations by Leya and Masarik (2009), a preatmospheric radius of somewhat above 200 cm is required to result in production rates in the interior becoming an order of magnitude below maximum values near the surface. The find mass of ~7000 kg of NWA 869 requires a conservative minimum radius of about 85 cm. Apparently, the true size of the preatmospheric meteoroid was even considerably larger and was strongly reduced by loss during atmospheric passage. Loss on the order of 90–95% of an r = 200 cm body would be sufficient to explain a total terminal mass of ~7000 kg. Such or even much larger loss fractions are not uncommon for big meteoroids. The estimated 4–6 t of surviving meteorites represents only ~0.03–0.05% of the preatmospheric mass of Chelyabinsk (Popova et al. 2013). In any case, we note that the nominal low cosmic ray exposure ages of cluster chondrite clast M-06-44-1-a have no physical

meaning. All other meteorites in this study have a find mass small enough that our assumption of similar shielding of all their studied samples is justified.

Radiogenic ^{4}He, ^{40}Ar, and ^{129}Xe

Table A3 shows the radiogenic portions of ^{4}He, ^{40}Ar, and ^{129}Xe* (from the decay of U-Th, K, and ^{129}I, respectively) for the samples for which these quantities can be determined with reasonable confidence. For ^{4}He, this is clearly impossible for the samples with very high concentrations of SW noble gases, but it may also be problematic for other samples that may contain sizeable concentrations of trapped ^{4}He. We therefore do not report radiogenic ^{4}He concentrations for these samples. Also the very low $^{4}He_{rad}$ concentrations stated for all samples of the probably paired NWA 5205, NWA 5421, and NWA 6742 should be viewed as upper limits (see the Samples and Methods section).

The main observations from Table A3 can be summarized as follows:

1. The three meteorites NWA 5205, NWA 5421, and NWA 6742 all have very low—concentrations of radiogenic ^{4}He, not exceeding 31×10^{-8} cm^{3}STP per g. In NWA 5205, cluster chondrite clasts and matrix samples show similarly low values. These concentrations correspond to nominal U-Th-^{4}He ages of some 110 Ma or lower, assuming U and Th concentrations in our samples as given for the respective meteorite groups by Lodders and Fegley (1998). All cluster chondrite clast samples of the meteorites NWA 869, NWA 2336, NWA 3119, NWA 5206, and NWA 6007 have $^{4}He_{rad}$ concentrations between $(675–854) \times 10^{-8}$ cm^{3}STP per g, corresponding to U-Th-He ages on the order of 2100–2500 Ma. No reliable comparison between ^{4}He ages in cluster chondrite clast and matrix samples in the same meteorite is possible for NWA 869, NWA 2336, and NWA 3119. All respective matrix samples certainly or possibly contain SW-He or primordial He impossible or difficult to correct for.
2. Concentrations of ^{40}Ar are also highly variable (see also Fig. A2). The by far lowest values are observed for the three meteorites that also show very low $^{4}He_{rad}$ concentrations (NWA 5205, NWA 5421, and NWA 6742). Adopting average K concentrations of LL chondrites (Lodders and Fegley 1998), nominal ^{40}K-^{40}Ar ages of these samples fall between ~300 and 1500 Ma. The other meteorites show nominal ages between ~2500 and 4600 Ma. No systematic difference in ^{40}Ar concentrations is observed between cluster chondrite clasts and matrix samples of the same meteorite (i) in NWA 869 and NWA 4522, matrix samples have roughly 35% lower values than cluster chondrite clasts; (ii) NWA 3119 shows more than two times as much ^{40}Ar in its matrix lithology than in its cluster chondrite clast samples; (iii) for NWA 2336, no significant difference is found between the two lithologies.
3. Concentrations of radiogenic ^{129}Xe* for most samples fall between ~$(0.5–1.4) \times 10^{-10}$ cm^{3}STP per g. In most cases, there are no systematic differences between cluster chondrite clast and matrix samples. However, both subsamples of cluster chondrite clast M-06-44-1-a (ccc a1 and ccc a2) contain about 20 times more ^{129}Xe* than the second cluster chondrite clast (ccc b) of this meteorite. Possible reasons for this are discussed in the Radiogenic Noble Gases section.
4. The simultaneously low ^{4}He and ^{40}Ar values of NWA 5205, NWA 5421, and NWA 6742 support the hypothesis noted in the Primordial Q Gases for Ar, Kr, and Xe in All Samples section that these three meteorites with similarly low ^{21}Ne exposure ages are paired.

DISCUSSION

This study aims to shed further light on the formation and evolution of UOCs containing cluster chondrite clasts. We do this mainly by evaluating possible differences or similarities in the noble gas records of cluster chondrite clast and matrix materials, respectively, with special emphasis—where possible—on comparisons of these two lithologies in the same meteorite. In the following, we will separately discuss trapped noble gases (primordial and SW-implanted gases); cosmic ray-produced noble gases; and radiogenic ^{4}He, ^{40}Ar, and ^{129}Xe.

Trapped Noble Gases

A clear dichotomy exists in the trapped He and Ne records of matrix and cluster chondrite clast lithologies (Tables 2 and 5). With the exception of NWA 5205, all matrix samples contain He and Ne implanted by the SW (Fig. 2), whereas the cluster chondrite clast samples are essentially devoid of SW noble gases (apart from some contamination with matrix material in NWA 869 sample M-06-44-1 noted in the Trapped He, Ne (and Ar) Implanted by the SW in Matrix Samples section). SW noble gases in a meteorite sample typically indicate an origin in a parent body regolith (Eberhardt et al. 1965; Wieler et al. 1989). Hence, most of the meteorites for which matrix samples were analyzed—and perhaps most or all of the others too—once resided in their parent body regolith. Impact "gardening" of lunar and asteroidal regoliths leads to efficient mixing so that most

individual grains once became irradiated by the SW at the immediate regolith surface. Welten et al. (2011) already concluded this for the large regolith breccia NWA 869. The lack of SW noble gases in the cluster chondrite clasts shows that they remained intact pebbles of primary accretionary rock during regolith gardening. It is common that SW-bearing ("gas-rich") chondrites are mixtures of fine-grained (usually "dark") matrix containing SW noble gases and "light" inclusions that are devoid of SW noble gases in their interior (e.g., Wieler et al. 1989). The same relation between clastic matrix and clasts of "primary accretionary rock" is found for CM chondrites by Nakamura et al. (1999). This relation is also supported by the observation that preirradiated olivine grains occur exclusively in the clastic matrix of these meteorites (Metzler 2004; Riebe et al. 2017a). Concentrations of SW ^{20}Ne in our matrix samples apart from NWA 5205 fall between (35–940) $\times$ 10^{-8}cm^{3}STP per g (Table 5), a range commonly observed in SW-rich ordinary chondrites (Schultz and Franke 2004). The highest concentration here is a factor of roughly 3–6 lower than values in the H chondrite Fayetteville (Wieler et al. 1989), one of the most gas-rich meteorites. The meteorites studied here can thus be qualified as submature to immature asteroidal regolith breccias. NWA 5205 appears to be a fragmental breccia, as even its matrix samples analyzed here are free of SW He and Ne.

As noted in the Primordial Q Gases for Ar, Kr, and Xe in All Samples section, the SW component is, however, negligible in the budget of the heavy noble gases Kr and Xe even in the matrix samples with the highest concentrations of SW He and Ne. Rather, all samples contain sizeable amounts of primordial Kr and Xe mainly from the Q component, though some atmospheric Xe and especially atmospheric Kr have affected the budget of the heavy noble gases, as is often the case for hot desert meteorites (Scherer et al. 1994). Primordial He and Ne are only—if at all—visible in the SW-free samples. Trapped Ar in the SW-gas-rich samples is a mixture of SW and Q components. Here, we will concentrate on the three heavy noble gases—in particular Xe—in the cluster chondrite samples, to study possible similarities and differences in the primordial noble gas records of these fast-accreted primary accretionary rocks and common unequilibrated L and LL chondrites.

Relative elemental abundances of the primordial gases in the (SW-free) cluster chondrite clast samples (Table 5) cover the same range as typical unequilibrated LL and L chondrites. There is thus no obvious difference in the mix of primordial noble gas components between the cluster chondrite clasts studied here and other UOCs. Figure 5 shows that cluster chondrite clasts also display the well-known trend of higher primordial Xe concentrations in UOCs of lower petrologic type (Anders and Zadnik 1985). On the left part of the figure, the LL chondrite samples are sorted along the abscissa according to their chemical class and petrologic type, with concentrations decreasing from ~45 $\times$ 10^{-10} cm^{3}STP per g to ~6 $\times$ 10^{-10} cm^{3}STP per g. This range compares well with the range of Xe concentrations of unequilibrated LL chondrites of various petrologic types (cf. Keil et al. 2015), which is also indicated in Fig. 5 by the dotted lines. This similarity may be remarkable, because the cluster chondrite clasts contain about two times lower fractions of fine-grained interchondrule materials than UOCs in general (Metzler 2012). Primordial noble gases in chondrites reside in fine-grained components (e.g., Vogel et al. 2003, 2004). Taken at face value, the fine-grained portions in cluster chondrite clasts, therefore, appear to show enhanced concentrations of primordial noble gas carriers (here in particular phase Q) relative to the fine-grained fractions of the LL chondrite samples shown for comparison. This conclusion may have to be taken with a grain of salt, since we cannot exclude that some of the literature analyses stem from samples also partly representing cluster chondrite lithologies. Some literature data may also be from samples similar to clastic matrix of this study, which may be of higher petrologic types, as discussed in the next paragraph. Yet, Leitner et al. (2014) observed remarkably high concentrations of presolar silicates in cluster chondrite clasts in two highly unequilibrated LL chondrites (Krymka and NWA 1756) relative to typical UOC values, including bulk Krymka. This observation is in line with a higher concentration of carriers of primordial noble gases in cluster chondrite clasts postulated here, as both Q gas concentration and presolar grain abundance in various meteorite classes correlate (Huss 1997). This implies an intimate mixing of phase Q and presolar dust in the solar nebula. Leitner et al. (2014) note that their observation indicates fast cooling after accretion, as the presolar dust in the fine-grained materials surrounding the chondrules would otherwise have been largely destroyed by melting and sintering processes. Possibly the fast accretion also (partly) suppressed initial degassing of phase Q and perhaps other primordial noble gas carriers, while gas loss during subsequent parent body metamorphism in the LL cluster chondrites was similar to that in unequilibrated LL chondrites in general.

The matrix samples are shown separately in the right part of Fig. 5, since the petrologic types of the meteorites as listed in Table 1 only apply to the respective cluster chondrite clasts. The matrix of an impact breccia usually contains a large variety of

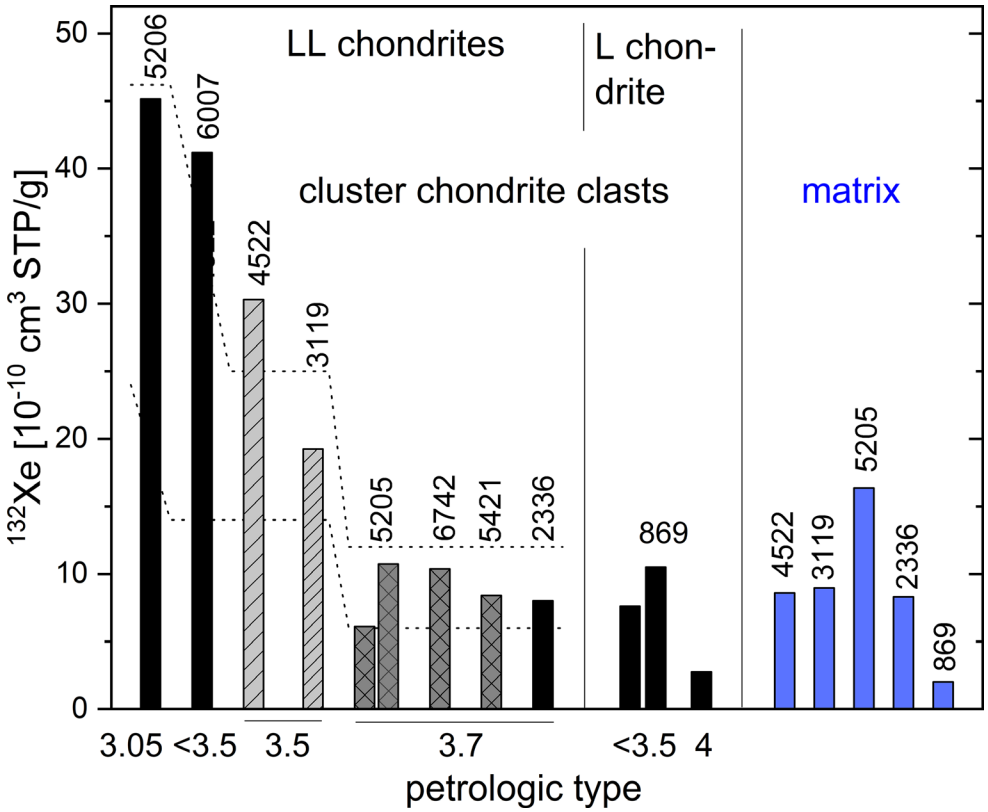

Fig. 5. Concentrations of trapped ^{132}Xe in cluster chondrite clasts and matrix samples measured in this work (Table 3). Meteorite names (without "NWA" prefix) given on top of bar groups. The two different gray patterns represent cluster chondrite clast samples of the two sets of paired or likely paired meteorites. Petrologic types of cluster chondrite clasts are indicated as abscissa labels. The dotted contours on the left part of the figure indicate typical concentration ranges of primordial Xe in LL chondrites of similar petrologic types as those of the cluster chondrite clasts analyzed in this work (cf. Keil et al. 2015). (Color figure can be viewed at wileyonlinelibrary.com.)

admixed components of different origin and may contain fragments from other sites/depths of the parent asteroid. If the matrix mixture is dominated by fragments of chondritic rocks of higher petrologic type (more strongly degassed) than a clast, then a lower concentration of trapped gases can be expected in the matrix (e.g., NWA 3119, NWA 4522). Also the opposite relation is possible (matrix dominated by components of lower petrologic type than the clast), and then, matrix is richer in trapped gases due to less degassed matrix components (e.g., NWA 5205). If a breccia matrix mostly consists of the same material as a cluster chondrite clast, comparable gas concentrations can be expected (e.g., NWA 2336). This assumption was checked for the latter sample by measuring the variation of chemical composition of olivines in clast and matrix. It turned out that the mean composition of olivine in the clast is $Fa_{27.9\pm8.3}$ (n = 31), nearly identical to the value for the clastic matrix ($Fa_{28.7\pm8.5;}$ n = 29). The percentage mean deviation of Fa values is 29.6 for both lithologies, which led to the petrologic subtype 3.7 (see Hutchison 2004; his table 2.6) of the clast in NWA 2336 (Table 1).

Cosmogenic Noble Gases

To evaluate possible differences in the exposure ages of cluster chondrite clast and matrix samples of the same meteorite, we first compare age values determined in different sample pairs of the same lithology in any given meteorite (Table 4). Among the 13 such pairs, 10 show differences in T21 values of 12% or less and the other two (NWA 4522 mx, NWA 5421 ccc) differ in T21 by 19% and 15%, respectively. Therefore, T21 values of different subsamples of the same meteorite scatter by not more than 15–20%. Neglecting the same two exceptions (NWA 4522 mx, NWA 5421 ccc), which clearly suffered cosmogenic ^{3}He loss, T3 values of most pairs agree within 10% (the only further exception NWA 3119 mx agrees within 16%). Several T38 values of the same pair of subsamples show larger differences, up to 47% in the case of NWA 5205ccc F. These

differences are very likely due to inhomogeneities in Ca concentrations, as noted above. Hence, we base the following reasoning mainly on T21.

Based on the reproducibility of T21 noted in the previous paragraph, we conclude that T21 differences between cluster chondrite clast and matrix samples of the same meteorite of >(15–20)% are relevant. They indicate that the respective lithology with a higher nominal age had experienced an exposure to energetic cosmic ray particles prior to the final compaction of the meteorite (Table 4; Fig. 4). The criterion of a >(15–20)% difference is clearly fulfilled for NWA 869, with the average T21 of the two mx samples exceeding the average T21 of the two ccc samples by 65%. Similar trends—although less pronounced—hold for NWA 3119 and NWA 4522: The average T21 of the two NWA 3119 matrix samples is 21% higher than the average NWA 3119 ccc value. For the SW gas-rich meteorite NWA 4522, average T21 in mx samples exceeds the ccc values by 17%. Expressed in concentrations of cosmogenic ^{21}Ne, the differences are quite similar in all three cases, with mx samples containing ~(1.2–1.8) × 10^{-8} cm^3STP per g more cosmogenic ^{21}Ne than the ccc samples of the same meteorite. Less clear is the situation for NWA 2336, with only one analysis of each lithology available: While the less reliable T38 of the matrix sample is almost a factor of two higher than the T38 of its cluster chondrite clast, the corresponding difference in T21 is only 11%. Finally, the two lithologies of NWA 5205 hardly show different exposure ages.

In summary, we conclude that for three of the five chondrites for which matrix and cluster chondrite clast data are available, there is clear—and for a further meteorite equivocal—evidence that the matrix samples contain excesses of cosmogenic noble gases relative to the cluster chondrite clasts. The most likely explanation for this is a precompaction exposure of matrix samples in the parent body regolith. This conclusion is also supported by the fact that NWA 5205 does not show a pre-exposure, as this is the only meteorite with matrix samples studied here which is likely not a regolith breccia but a fragmental breccia (e.g., Bischoff et al. 2006). The $^{21}Ne_{cos}$ excesses of NWA 869, NWA 3119, and NWA 4522 would correspond to exposure ages on the order of 6–10 Ma in near surface regions of a parent body in 2π exposure geometries. Unfortunately, due to the presence of SW-Ne, the shielding parameter $(^{22}Ne/^{21}Ne)_{cos}$ could not be determined for matrix samples of any of the four meteorites for which a precompaction exposure of the matrix portions is certain or possible. Hence, no inferences about shielding conditions during pre-exposure are possible. All samples of the one meteorite with no signs of a pre-exposure—NWA 5205—show very similar $(^{22}Ne/^{21}Ne)_{cos}$ ratios, as expected.

Welten et al. (2011) already concluded, based on cosmogenic noble gases and radionuclides, that some of their samples of NWA 869 had experienced parent body exposures, on the order of 10–30 Ma. Note that Welten et al. (2011) derive a 4π exposure age of NWA 969 of 5 ± 1 Ma, based on ^{21}Ne and ^{26}Al. This age range agrees with the T21 values of our two cluster chondrite clast samples of this meteorite (6.0 and 5.3 Ma, Table 4), although the $^{21}Ne_{cos}$ concentrations of the samples by Welten et al. (2011) are several times lower than those determined here. This can be explained by a considerably higher shielding of the samples studied by Welten et al. (2011) compared to ours, consistent with the large mass of the NWA 869 meteoroid.

Radiogenic Noble Gases

No concentrations for the parent elements U, Th, and K of radiogenic ^{4}He and ^{40}Ar for individual samples analyzed here are available. We therefore adopt average U, Th, and K concentrations for the respective meteorite groups (Wasson and Kallemeyn 1988; Lodders and Fegley 1998).

As noted in the Results section, the three meteorites NWA 5205, NWA 5421, and NWA 6742 all have very low concentrations of radiogenic ^{4}He and ^{40}Ar, resulting in nominal U/Th-^{4}He ages (or their upper limits) of between 20 and 110 Ma and K-^{40}Ar ages of between 310 and 1080 Ma. This indicates that these three likely paired LL chondrites suffered a severe loss of ^{4}He and ^{40}Ar probably not earlier than 20 Ma ago, possibly coinciding with the impact that triggered the cosmic ray exposure clock of these meteorites some 2.5 Ma ago. The other samples yield nominal U/Th-^{4}He ages (if available) between about 2100 and 2950 Ma and nominal K-Ar ages between ~2500 and 4600 Ma. Our range of K-Ar ages for NWA 869 of 3700–4430 Ma agrees well with the age range of 3.3–4.4 Ga reported by Welten et al. (2011). Also, our U/Th-^{4}He ages of the two cluster chondrite clast b samples of 2400 and 2950 Ma, respectively, are consistent with the value of 2.83 Ga reported for NWA 869 by these authors. Metzler et al. (2011) reported a more detailed ^{39}Ar-^{40}Ar age study on several NWA 869 samples (different from those studied here) and identified different impact heating events between 4402 and 1790 Ma. These authors note that NWA 869 therefore escaped the large impact event on the L chondrite parent body some 470 Ma ago, which reset the K-Ar clock of a large fraction of the L chondrites (Korochantseva et al. 2007).

Do we see significant differences in noble gas retention ages between the two different lithologies studied here? For ^{4}He, this question cannot be addressed here, since a concentration of radiogenic ^{4}He

in a matrix sample is available only for one meteorite (NWA 5205) due to the presence of $^4He_{SW}$ in all other samples. NWA 5205 belongs to the group that suffered a severe recent loss of ^4He (and ^{40}Ar). The nominal, already very low $^4He_{rad}$ values for the NWA 5205 samples have to be considered as upper limits. In the case of ^{40}Ar, two meteorites (NWA 869 and NWA 4522) show higher nominal K-Ar ages for the cluster chondrite clasts than for the matrix, whereas the opposite trend is observed for NWA 3119. For NWA 2336 and NWA 5205, no unequivocal difference is visible. The differences in ^{40}Ar concentrations displayed by NWA 869, NWA 4522, and NWA 3119 seem to be robust, as they are documented in all three cases with two analyses of each lithology. We are nevertheless reluctant to firmly conclude that these concentration differences really imply differences in ^{40}Ar retention ages, since we have no information about the true K concentrations of any of our samples. Potassium concentrations can significantly vary in aliquots of typically 10–20 mg of the same meteorite (Di Gregorio et al. 2019). Metzler et al. (2011) noted, for example, that some clasts of NWA 869 contain several times more K than typical L chondrite bulk samples.

With one exception, all samples contain concentrations of radiogenic $^{129}Xe^*$ in the range of $(0.5–1.4) \times 10^{-10}$ cm^3STP per g (Table A3; Fig. A1), similar to the values already observed for NWA 869 by Welten et al. (2011). For three of the five meteorites for which data for matrix samples are available, there is no substantial difference between mx and ccc samples of the same meteorite. The two exceptions are NWA 4522 and NWA 869. The cluster chondrite clast sample of NWA 4522 has a six times higher $^{129}Xe^*$ concentration than the respective matrix sample. This sample also contains ~3.5 times less ^{132}Xe than the analyzed cluster chondrite clast of NWA 4522; hence, this cluster chondrite clast may have retained trapped and radiogenic Xe better than its respective clastic matrix. If so, the cluster chondrite clast of NWA 4522 would also have retained radiogenic $^{129}Xe^*$ better than the analyzed cluster chondrite clast of NWA 3119, although these meteorites are likely paired. A possible explanation is that cluster chondrite clasts of different petrologic types may be present in the same breccia. Alternative explanations are that two cluster chondrite clasts likely from within the same meteoroid closed their I-Xe systems millions of years apart or had widely different iodine concentrations, but we consider these alternatives to be rather unlikely. The other exception (NWA 869) is also remarkable. Both subsamples of cluster chondrite clast M-06-44-1-a (ccc a1 and ccc a2) contain about 20 times more $^{129}Xe^*$ than the other analyzed cluster chondrite clast (ccc b) of this meteorite. The latter sample is of petrologic type 4, which is also reflected by its about three times lower trapped Xe concentration compared to ccc a. A protracted closure of the I-Xe system and later Xe loss on the parent body may thus explain the much lower $^{129}Xe^*$ of ccc b.

CONCLUSIONS

This work presents a comparative study of the noble gas records in two different lithologies of a series of UOC finds from Northwest Africa: cluster chondrite clasts and clastic matrix ("matrix") samples. Cluster chondrite clasts are characterized by close-fit textures of deformed and indented chondrules, indicating compaction of hot chondrules within hours or days after formation. The resulting rocks became fragmented on a parent body by secondary impacts and mixed with isolated chondrules, chondrule fragments, small rock fragments containing "normal" spheroidal chondrules, and fine-grained impact-induced dust, that is, the present-day clastic matrix lithology (Metzler 2012).

The noble gas characteristics of the two different lithologies show two major differences. First, the matrix samples of most of the studied meteorites contain noble gases from the SW, clearly visible in their concentrations and isotopic compositions of Ne (and mostly also He). Cluster chondrite clast samples are devoid of SW noble gases (with one exception likely caused by some contamination with matrix material). Second, matrix samples of several meteorites contain substantially larger concentrations of cosmogenic noble gases than their corresponding cluster chondrite clasts, indicating an exposure of the matrix materials in the surface regolith of their parent asteroids on the order of a few up to around 10 million years. The Xe and Kr records of all samples of both lithologies are dominated by primordial noble gases (mostly the Q component), with minor contamination by atmospheric Xe and somewhat larger atmospheric Kr contributions. The primordial Xe concentrations of the cluster chondrite clasts clearly decrease with increasing grade of thermal metamorphism, as is common for chondrites (Anders and Zadnik 1985).

The dichotomy between the SW-bearing matrix samples and the SW-free cluster chondrite clasts confirms the conclusion that the latter are fragments of "primary accretionary rocks" (Metzler 2012). The cluster chondrite clasts were mixed into matrix matter reworked in a parent body regolith whose fine-grained constituents had trapped SW noble gases. One of the five studied meteorites (NWA 5205) appears not to derive from an asteroid regolith, as both subsamples of its matrix lithology are devoid of SW He and Ne. This meteorite and its two probable pairings NWA 5421 and NWA 6742 represent a fragmental breccia. The excesses of cosmogenic noble gases in matrix samples relative to

the respective cluster chondrite clast values are in agreement with the above picture. Matrix samples were irradiated by GCRs in their parent body regolith, whereas probably most or all cosmogenic noble gases in the cluster chondrite clast samples were produced during the 4π exposure stages of the respective meteorites. Regolith pre-exposure durations of several million years as observed in this work are typical for asteroidal regoliths (Wieler et al. 1989). For NWA 869, the 4π ^{21}Ne exposure age of ~5–6 Ma determined here is identical to the value reported by Welten et al. (2011) based on ^{21}Ne-^{26}Al systematics. These authors also derive parent body pre-exposure ages of up to several 10 Ma for some of their NWA 869 samples. Some samples from this very large meteorite must stem from its interior, making shielding corrections for cosmogenic noble gas production rates unreliable.

Primordial Xe concentrations of the cluster chondrite clasts of the LL chondrites compare well with those of other LLs of similar petrologic types (e.g., Keil et al. 2015). This is rather remarkable, as the cluster chondrite clasts contain substantially lower fractions of trapped noble gas-bearing fine-grained interchondrule materials reported for typical unequilibrated LL chondrites. This observation is in line with the relatively high abundance of presolar silicates in cluster chondrite clasts (Leitner et al. 2014) and may suggest that the fast formation of the primary accretionary rocks represented by cluster chondrite clasts suppressed initial degassing of their trapped noble gas carriers.

The noble gas data strongly indicate that the three meteorites NWA 5205, NWA 5421, and NWA 6742 are paired. Also, NWA 3119 and NWA 4522 are likely paired.

Acknowledgments—K. Müsing and H. Busemann acknowledge advice and support in the laboratory by Maïa Kuga, Patrizia Will, and Daniela Krietsch. We appreciate the helpful comments by G. Avice and an anonymous reviewer. K. Metzler acknowledges financial support by the German Research Foundation (DFG) within the Priority Program "The First 10 Million Years of the Solar System—a Planetary Materials Approach" (SPP 1385; ME 1115/8). This work has partly (M. Riebe and H. Busemann) been carried out within the framework of the NCCR (National Centre of Competence in Research) "PlanetS" supported by the Swiss National Science Foundation.

Data Availability Statement—All noble gas data reported here are available at the ETH repository: https://doi.org/10.3929/ethz-b-000467535

Editorial Handling—Dr. Yves Marrocchi

REFERENCES

Alexeev V. A. 1998. Parent bodies of L and H chondrites: Times of catastrophic events. *Meteoritics & Planetary Science* 33:145–152.

Anders E. and Zadnik M. G. 1985. Unequilibrated ordinary chondrites: A tentative subclassification based on volatile-element content. *Geochimica et Cosmochimica Acta* 49:1281–1291.

Bekaert D. V., Marrocchi Y., Meshik A., Remusat L., and Marty B. 2019. Primordial heavy noble gases in the pristine Paris carbonaceous chondrite. *Meteoritics & Planetary Science* 54:395–414.

Bischoff A., Scott E. R. D., Metzler K., and Goodrich C. A. 2006. Nature and origins of meteoritic breccias. In *Meteorites and the early solar system II*, edited by Lauretta D. S. and McSween H. Y. Tucson, Arizona: The University of Arizona Press. pp. 679–712.

Bischoff A., Schleiting M., Wieler R., and Patzek M. 2018. Brecciation among 2280 ordinary chondrites—Constraints on the evolution of their parent bodies. *Geochimica et Cosmochimica Acta* 238:516–541.

Busemann H., Baur H., and Wieler R. 2000. Primordial noble gases in "phase Q" in carbonaceous and ordinary chondrites studied by closed-system stepped etching. *Meteoritics & Planetary Science* 35:949–973.

David J. C. and Leya I. 2019. Spallation, cosmic rays, meteorites, and planetology. *Progress in Particle and Nuclear Physics* 109:103711.

Di Gregorio M., Busemann H., Hunt A. C., Krietsch D., Schönbächler M., and Maden C. 2019. Variable cosmogenic argon in L/LL5 chondrite Knyahinya (abstract #2157). 82nd Annual Meeting of the Meteoritical Society. *Meteoritics & Planetary Science* 54.

Eberhardt P., Geiss J., and Grögler N. 1965. Further evidence on the origin of trapped gases in the meteorite Khor Temiki. *Journal of Geophysical Research* 70:4375–4378.

Grimberg A., Baur H., Bochsler P., Bühler F., Burnett D. S., Hays C. C., Heber V. S., Jurewicz A. J. G., and Wieler R. 2006. Solar wind neon from Genesis: Implications for the lunar noble gas record. *Science* 314:1133–1135.

Heber V. S., Wieler R., Baur H., Olinger C., Friedmann T. A., and Burnett D. S. 2009. Noble gas composition of the solar wind as collected by the Genesis mission. *Geochimica et Cosmochimica Acta* 73:7414–7432.

Herzog G. F. and Caffee M. W. 2014. Cosmic-ray exposure ages of meteorites. In *Meteorites and cosmochemical processes*, edited by Davis A. M. Treatise on Geochemistry, vol. 1. Amsterdam: Elsevier. pp. 419–454.

Huber L., Metzler K., Maden C., and Wieler R. 2013. Noble gases in cluster chondrite clasts. 76th annual Meeting of the Meteoritical Society. *Meteoritics & Planetary Science* 48.

Huss G. R. 1997. The survival of presolar grains in solar system bodies. In *Astrophysical implications of the laboratory study of presolar materials*, edited by Bernatowicz T. J. and Zinner E. AIP Conference Proceedings 402. New York: American Institute of Physics. pp. 721–748.

Hutchison R. 2004. Meteorites—A petrologic, chemical and isotopic synthesis. In *Cambridge planetary science*, edited by Bagenal F., Jewitt D., Murray C., Bell J., Lorenz R., Nimmo F. and Russell S. Cambridge, UK: Cambridge University Press. 506 p.

Hyde B. C., Tait K. T., Moser D. E., Rumble D., and Thompson M. S. 2020. Accretionary mixing of a eucrite

impactor and the regolith of the L chondrite parent body. *Meteoritics & Planetary Science* 55:20–35.

Keil K., Zucolotto M. E., Krot A. N., Doyle P. M., Telus M., Krot T. V., Greenwood R. C., Franchi I. A., Wasson J. T., Welten K. C., Caffee M. W., Sears D. W. G., Riebe M., Wieler R., dos Santos E., Scorzelli R. B., Gattacceca J., Lagroix F., Laubenstein M., Mendes J. C., Schmitt-Kopplin P., Harir M., and Moutinho A. L. R. 2015. The Vicencia meteorite fall: A new unshocked (S1) weakly metamorphosed (3.2) LL chondrite. *Meteoritics & Planetary Science* 50:1089–1111.

Kööp L., Heck P. R., Busemann H., Davis A. M., Greer J., Maden C., Meier M. M. M., and Wieler R. 2018. High early solar activity inferred from helium and neon excesses in the oldest meteorite inclusions. *Nature Astronomy* 2:709–713.

Korochantseva E. V., Trieloff M., Lorenz C. A., Buykin A. I., Ivanova M. A., Schwarz W. H., Hopp J., and Jessberger E. K. 2007. L-chondrite asteroid breakup tied to Ordovician meteorite shower by multiple isochron Ar-40-Ar-39 dating. *Meteoritics & Planetary Science* 42:113–130.

Leitner J., Metzler K., and Hoppe P. 2014. Characterization of presolar grains in cluster chondrite clasts from unequilibrated ordinary chondrites (abstract #1099). 45th Lunar and Planetary Science Conference. CD-ROM.

Leya I. and Masarik J. 2009. Cosmogenic nuclides in stony meteorites revisited. *Meteoritics & Planetary Science* 44:1061–1086.

Lodders K. and Fegley B. 1998. *The planetary scientist's companion*. New York: Oxford University Press. 371 pp.

Mathew K. J. and Marti K. 2003. Solar wind and other gases in the regoliths of the Pesyanoe parent object and the moon. *Meteoritics & Planetary Science* 38:627–643.

Meteoritical Bulletin Database. https://www.lpi.usra.edu/meteor/metbull.php. Accessed November 14, 2020.

Metzler K. 2004. Formation of accretionary dust mantles in the solar nebula: Evidence from preirradiated olivines in CM chondrites. *Meteoritics & Planetary Science* 39:1307–1319.

Metzler K., Bischoff A., Greenwood R. C., Palme H., Gellissen M., Hopp J., Franchi I. A., and Trieloff M. 2011. The L3–6 chondritic regolith breccia Northwest Africa (NWA) 869: (I) Petrology, chemistry, oxygen isotopes, and Ar-Ar age determinations. *Meteoritics & Planetary Science* 46:652–680.

Metzler K. 2012. Ultrarapid chondrite formation by hot chondrule accretion? Evidence from unequilibrated ordinary chondrites. *Meteoritics & Planetary Science* 47:2193–2217.

Metzler K. and Pack A. 2016. Chemistry and oxygen isotopic composition of cluster chondrite clasts and their components in LL3 chondrites. *Meteoritics & Planetary Science* 51:276–302.

Metzler K., Hezel D. C., and Nellesen J. 2019. Various size-sorting processes for millimeter-sized particles in the Sun′s protoplanetary disk? Evidence from chondrules in ordinary chondrites. *Astrophysical Journal* 887:230. https://doi.org/10.3847/1538-4357/ab58d0

Nakamura T., Nagao K., Metzler K., and Takaoka N. 1999. Heterogeneous distribution of solar and cosmogenic noble gases in CM chondrites and implications for the formation of CM parent bodies. *Geochimica et Cosmochimica Acta* 63:257–273.

Osawa T. and Nagao K. 2006. Noble gases in solar gas–rich and solar-gas-free polymict breccias. *Antarctic Meteorite Research* 19:58–78.

Ott U. 2014. Planetary and pre-solar noble gases in meteorites. *Chemie der Erde (Geochemistry)*. 74:519–544.

Pedroni A. and Begemann F. 1994. On unfractionated solar noble gases in the H3–6 meteorite Acfer111. *Meteoritics* 29:632–642.

Popova O. P., Jenniskens P., Emel'yanenko V., Kartashova A., Biryukov E., Khaibrakhmanov S., Shuvalov V., Rybnov Y., Dudorov A., Grokhovsky V. I., Badyukov D. D., Yin Q. Z., Gural P. S., Albers J., Granvik M., Evers L. G., Kuiper J., Kharlamov V., Solovyov A., Rusakov Y. S., Korotkiy S., Serdyuk I., Korochantsev A. V., Larionov M. Y., Glazachev D., Mayer A. E., Gisler G., Gladkovsky S. V., Wimpenny J., Sanborn M. E., Yamakawa A., Verosub K. L., Rowland D. J., Roeske S., Botto N. W., Friedrich J. M., Zolensky M. E., Le L., Ross D., Ziegler K., Nakamura T., Ahn I., Lee J. I., Zhou Q., Li X. H., Li Q. L., Liu Y., Tang G. Q., Hiroi T., Sears D., Weinstein I. A., Vokhmintsev A. S., Ishchenko A. V., Schmitt-Kopplin P., Hertkorn N., Nagao K., Haba M. K., Komatsu M., and Mikouchi T. 2013. Chelyabinsk airburst, damage assessment, meteorite recovery, and characterization. *Science* 342:1069–1073.

Riebe M. E. I., Huber L., Metzler K., Busemann H., Luginbuehl S. M., Meier M. M. M., Maden C., and Wieler R. 2017a. Cosmogenic He and Ne in chondrules from clastic matrix and a cluster chondrite clast of Murchison: No pre-irradiation by the early sun. *Geochimica et Cosmochimica Acta* 213:618–634.

Riebe M. E. I., Welten K. C., Meier M. M. M., Wieler R., Barth M. I. F., Ward D., Bischoff A., Caffee M. W., Nishiizumi K., and Busemann H. 2017b. Cosmic-ray exposure ages of six chondritic Almahata Sitta fragments. *Meteoritics & Planetary Science* 52:2353–2374.

Scherer P., Schultz L., and Loeken T. 1994. Weathering and atmospheric noble gases in chondrites. In *Noble gas geochemistry and cosmochemistry*, edited by Matsuda J. Tokyo: Terra Scientific Publishing Company (Terrapub). pp. 43–53.

Schultz L. and Franke L. 2004. *Helium, neon, and argon in meteorites—A data collection*. Mainz: Max-Planck-Institut für Chemie. CD-ROM.

Scott E. R. D. 1984. Classification, metamorphism, and brecciation of type 3 chondrites from Antarctica. *Smithsonian Contributions to the Earth Sciences* 26:73–93.

Scott E. R. D. and Taylor G. J. 1982. Primitive breccias among the type 3 ordinary chondrites—Origin and relation to regolith breccias. In *Workshop on lunar breccias and soils and their meteoritic analogs*, edited by Taylor G. J. and Wilkening L. L. LPI Technical Report 82-02. Houston, Texas: Lunar and Planetary Institute. pp. 130–134.

Vogel N., Wieler R., Bischoff A., and Baur H. 2003. Microdistribution of primordial Ne and Ar in fine-grained rims, matrices, and dark inclusions of unequilibrated chondrites—Clues on nebular processes. *Meteoritics & Planetary Science* 38:1399–1418.

Vogel N., Leya I., Bischoff A., Baur H., and Wieler R. 2004. Noble gases in chondrules and associated metal-sulfide-rich samples: Clues on chondrule formation and the behavior of noble gas carrier phases. *Meteoritics & Planetary Science* 39:117–135.

Wasson J. T. and Kallemeyn G. W. 1988. Composition of chondrites. *Philosophical Transactions of the Royal Society of London A* 325:535–544.

Weisberg M. K., McCoy T. J., and Krot A. N. 2006. Systematics and evaluation of meteorite classification. In *Meteorites and the early solar system II*, edited by Lauretta D. S. and McSween H. Y. Tucson, Arizona: The University of Arizona Press. pp. 431–459.

Welten K., Caffee M. W., Franke L., Jull A. J. T., LeClerc M. D., Metzler K., and Ott U. 2011. The L3–6 chondritic regolith breccia Northwest Africa (NWA) 869: (II) Noble gases and cosmogenic radionuclides. *Meteoritics & Planetary Science* 46:970–988.

Wieler R. 2002a. Cosmic-ray-produced noble gases in meteorites. *Reviews in Mineralogy and Geochemistry* 47:125–170.

Wieler R. 2002b. Noble gases in the solar system. *Reviews in Mineralogy and Geochemistry* 47:21–70.

Wieler R. 2016. Do lunar and meteoritic archives record temporal variations in the composition of solar wind noble gases and nitrogen? A reassessment in the light of Genesis data. *Chem Erde-Geochemistry* 76:463–480.

Wieler R., Baur H., Pedroni A., Signer P., and Pellas P. 1989. Exposure history of the regolithic chondrite Fayetteville: I. Solar-gas-rich matrix. *Geochimica et Cosmochimica Acta* 53:1441–1448.

Wieler R., Busemann H., and Franchi I. A. 2006. Trapping and modification processes of noble gases and nitrogen in meteorites and their parent bodies. In *Meteorites and the early solar system II*, edited by Lauretta D. S. and McSween H. Y. Tucson, Arizona: The University of Arizona Press. pp. 499–521.

APPENDIX

Table A1. Kr isotopic ratios (^{84}Kr = 100) and ^{84}Kr/^{132}Xe.

	Lithol.	^{78}Kr	±	^{80}Kr	±	^{82}Kr	±	^{83}Kr	±	^{86}Kr	±	^{84}Kr/^{132}Xe	±
NWA 869	ccc a1	0.657	0.058	5.38	0.33	20.99	0.69	20.59	0.45	30.6	1.0	1.31	0.21
	ccc a2	0.587	0.016	4.97	0.05	20.48	0.13	20.02	0.13	30.7	0.2	0.98	0.04
	ccc b	0.615	0.088	10.40	0.68	22.2	1.09	20.56	0.93	29.8	1.4	0.85	0.14
	mx	0.690	0.178	6.57	0.57	22.1	1.8	20.7	1.7	29.3	2.5	1.20	0.21
NWA 2336	ccc	0.621	0.010	4.22	0.05	20.30	0.17	20.30	0.19	31.4	0.3	1.09	0.03
	mx	0.594	0.005	4.25	0.05	20.08	0.19	20.17	0.19	31.6	0.5	1.13	0.03
NWA 3119	ccc	0.631	0.057	4.09	0.25	20.16	0.67	19.51	0.41	29.2	1.0	1.39	0.22
	mx	0.716	0.065	4.74	0.29	21.02	0.71	20.92	0.41	29.9	1.0	1.55	0.24
NWA 4522	ccc	0.681	0.061	4.62	0.28	21.42	0.67	20.59	0.34	30.8	1.0	1.43	0.22
	mx	0.698	0.062	4.67	0.28	20.49	0.68	20.13	0.40	29.8	1.0	1.41	0.22
NWA 5205	ccc F	0.607	0.014	3.90	0.08	20.16	0.48	19.23	0.41	30.6	0.7	1.02	0.03
	ccc P	0.658	0.029	3.94	0.05	20.35	0.49	20.40	0.44	30.2	0.4	1.54	0.05
	mx	0.609	0.013	3.97	0.07	20.22	0.24	19.87	0.24	31.2	0.3	1.08	0.03
NWA 5206	ccc	0.680	0.060	4.34	0.26	21.18	0.67	20.78	0.38	30.6	1.0		
NWA 5421	ccc	0.641	0.060	4.26	0.26	20.96	0.71	21.50	0.53	30.7	1.0	1.42	0.22
NWA 6007	ccc	0.616	0.007	4.27	0.04	20.81	0.24	20.78	0.21	31.3	0.3	1.03	0.03
NWA 6742	ccc	0.678	0.078	4.29	0.28	20.64	0.83	20.20	0.66	30.2	1.2	1.08	0.13

Uncertainties (1σ) include ion counting statistics, mass discrimination, and spectrometer sensitivity variations. For "ccc" and "mx," see Table 1.

Table A2. Xe isotopic ratios (^{132}Xe = 100).

NWA #	Lith.	^{124}Xe	±	^{126}Xe	±	^{128}Xe	±	^{129}Xe	±	^{130}Xe	±	^{131}Xe		^{134}Xe		^{136}Xe	
869	ccc a1	0.479	0.015	0.432	0.011	8.41	0.10	450.7	10.0	16.77	0.20	84.2	1.0	39.10	0.56	33.15	0.46
	ccc a2	0.449	0.006	0.401	0.005	8.22	0.08	375.1	2.9	16.09	0.14	82.7	0.8	37.68	0.36	31.95	0.29
	ccc b	0.438	0.026	0.433	0.022	8.19	0.24	150.9	4.2	15.78	0.49	81.6	2.4	38.1	1.2	32.53	0.96
		0.394	0.007	0.353	0.007	7.36	0.09	113.9	1.5	15.44	0.17	79.5	0.9	38.80	0.43	33.05	0.40
	mx	0.519	0.053	0.380	0.040	8.22	0.76	142.1	11.8	16.37	1.51	82.6	7.5	38.6	3.7	31.7	2.8
2336	ccc	0.491	0.023	0.415	0.017	8.48	0.19	111.3	1.9	16.16	0.26	81.0	1.2	37.40	0.60	32.02	0.54
	mx	0.425	0.011	0.387	0.010	7.87	0.12	111.5	2.1	16.01	0.28	78.7	1.0	38.02	0.62	31.38	0.43
3119	ccc	0.431	0.009	0.424	0.013	8.21	0.15	112.9	2.2	16.58	0.24	83.3	1.2	39.35	0.74	32.57	0.48
	mx	0.419	0.011	0.403	0.014	7.70	0.15	116.0	2.0	15.54	0.28	79.5	1.7	37.81	0.88	30.86	0.54
4522	ccc	0.427	0.008	0.404	0.007	8.64	0.20	126.0	1.1	15.80	0.12	80.5	0.6	37.79	0.35	32.07	0.32
	mx	0.458	0.009	0.447	0.012	8.41	0.14	121.3	2.1	16.69	0.20	85.2	0.9	39.92	0.47	33.24	0.39
5205	ccc F	0.447	0.014	0.400	0.012	8.09	0.08	116.7	1.5	16.16	0.22	80.4	0.8	37.53	0.54	31.63	0.40
	ccc P	0.473	0.018	0.402	0.010	8.44	0.25	112.6	2.8	16.46	0.36	83.5	1.7	40.83	0.91	33.13	0.85
	mx	0.453	0.014	0.409	0.015	7.91	0.12	110.1	2.0	15.98	0.22	81.5	1.2	37.88	0.54	31.42	0.45
5206	ccc	0.457	0.009	0.420	0.009	8.37	0.11	107.7	2.2	16.63	0.21	84.5	1.1	39.30	0.56	33.04	0.42
5421	ccc	0.442	0.011	0.380	0.010	7.93	0.16	109.5	2.6	15.73	0.31	80.0	1.4	37.99	0.69	31.71	0.57
6007	ccc	0.422	0.010	0.376	0.009	7.77	0.14	104.5	2.2	15.58	0.26	79.7	1.3	37.75	0.64	31.66	0.55
6742	ccc	0.437	0.015	0.412	0.019	7.96	0.21	118.1	3.0	16.18	0.43	80.5	1.9	38.9	1.2	33.05	0.79

Uncertainties (1σ) include ion counting statistics, mass discrimination, and spectrometer sensitivity variations. For "ccc" and "mx," see Table 1.

Table A3. Radiogenic ^{4}He, ^{40}Ar, and ^{129}Xe*.

NWA #	Lith.	$^4He_{rad}$	$^{40}Ar_{rad}$	±	^{129}Xe*
869	ccc a1	748	6005	75	26.1
	ccc a2		4310	55	28.5
	ccc b	804	5560	450	1.25
		1054[a]			
	mx		3920	120	0.75
2336	ccc	800	2640	20	0.6
	mx		2465	20	0.7
3119	ccc	675	1675	20	1.2
	mx		4505	40	1.2
4522	ccc		5805	65	6.6
	mx		4360	110	1.1
5205	ccc F	6	106	5	0.8
	ccc P	31	461	46	0.5
	mx	24	180	10	1.0
5206	ccc	810	2585	20	
	ccc	744	3690	45	
5421	ccc	11	185	7	0.5
6007	ccc	854	4855	190	
6742	ccc	7	185	3	1.3

Concentrations of radiogenic ^{4}He and ^{40}Ar in (10^{-8} cm^{3}STP per g), concentrations of ^{129}Xe* in (10^{-10} cm^{3}STP per g). Values of $^4He_{rad}$ may have to be considered as upper limits, as no correction for possibly present trapped ^{4}He has been made. Concentrations of $^{40}Ar_{rad}$ are assumed to be equal to measured values, $^4He_{rad}$ and ^{129}Xe* calculated as explained in text.

For "ccc" and "mx," see Table 1.

[a]Initial analysis (see the Results section).

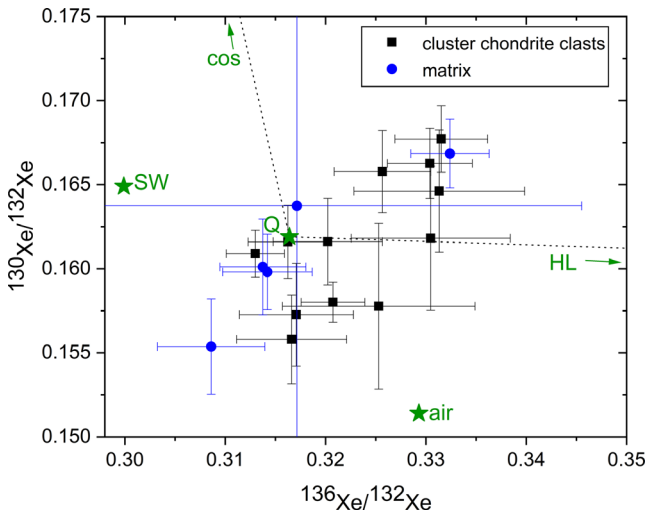

Fig. A1. Xe three-isotope diagram of cluster chondrite clast and matrix samples. Xe-Q (Busemann et al. 2000) and terrestrial atmospheric Xe compositions are indicated by green stars. Cosmogenic Xe in chondrites (Wieler 2002a) and Xe-HL (Ott 2014) plot far off scale. (Color figure can be viewed at wileyonlinelibrary.com.)

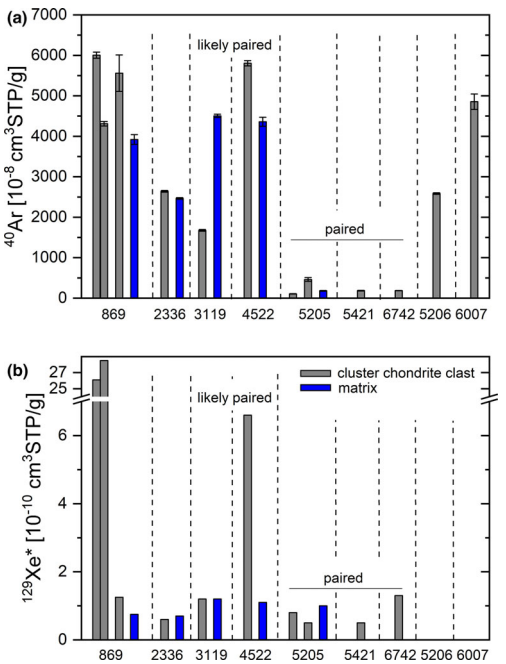

Fig. A2. a) Concentration of ^{40}Ar, assumed to be entirely radiogenic from decay of ^{40}K. b) Concentration of radiogenic ^{129}Xe* from decay of extinct ^{129}I. Abscissa labels represent meteorite names without the prefix "NWA." (Color figure can be viewed at wileyonlinelibrary.com.)